ETH IPP
Institute for Particle Physics

ETHZ-IPP Internal Report 2002-04
June 2002

Development of a z-vertex trigger based on drift chamber signals at H1

Niklaus E. Berger

Diploma thesis

supervised by
Prof. Dr. R. A. Eichler

Tutor: Dr. A. Schöning

Institute for Particle Physics
ETH - Zürich

Switzerland

July 15th 2002

Abstract

In the first part of this diploma thesis a z-vertex trigger based on drift chamber signals at H1 is studied. It is shown that such a trigger is feasible within the level 1 trigger latency of $2.2\,\mu$s and is rather easily implemented making use of the framework of the new Fast Track Trigger (FTT). Detailed simulations show that a z-vertex resolution of $\approx 6\,$cm can be obtained. Trigger efficiencies reach 99%, whilst at the same time $\approx$ 80% of the background events with tracks can be rejected.

The second part of this thesis is concerned with the development of a more accurate z-vertex determination on the second trigger level, based on the same drift chamber information that is used by the FTT. An algorithm based on already linked track segments is presented here, which reaches a resolution of $\approx$ 2 cm without requiring additional hardware.

Zusammenfassung

Im ersten Teil der vorliegenden Diplomarbeit wird ein z-Vertex-Trigger basierend auf Driftkammersignalen bei H1 studiert. Es wird gezeigt, daß es mit kleinem Aufwand möglich ist, einen solchen Trigger zu bauen, der innerhalb der Latenzzeit der ersten Triggerstufe von $2.2\,\mu$s eine Entscheidung fällen kann, wenn man ihn in den neuen schnellen Spurtrigger (FTT) einbettet. Eine detaillierte Simulation zeigt, daß der z Vertex auf $\approx 6\,$cm genau aufgelöst werden kann. Die Effizienz des Triggers erreicht 99%, während ca. 80% der Untergrundereignisse die Spuren enthalten, verworfen werden können.

Der zweite Teil dieser Arbeit dreht sich um eine verfeinerte z-Vertex Bestimmung auf der zweiten Triggerstufe unter ausschließlicher Benutzung der Driftkammerinformation, die auch der FTT verwendet. Es wird ein Algorithmus vorgestellt, der ohne zusätzliche Hardware zu benötigen, eine Vertex-Auflösung von $\approx$ 2 cm erreicht, indem er bereits gelinkte Spursegmente verwendet.

Contents

1 Introduction: Aim of this work **7**
1.1 A level 1 z-vertex trigger . . . 7
1.2 A refined z-vertex determination for the Level 2 FTT . . . 8

2 H1 at HERA **9**
2.1 The HERA storage ring . . . 9
2.2 The HERA II luminosity upgrade . . . 9
2.3 The H1 detector . . . 10
2.3.1 Overview . . . 10
2.3.2 Trigger . . . 11

3 The Fast Track Trigger **15**
3.1 Motivation . . . 15
3.2 The Central Jet Chamber . . . 15
3.3 The level 1 system . . . 16
3.3.1 Digitisation . . . 16
3.3.2 Track segment finding . . . 18
3.3.3 Track segment linking . . . 19
3.4 The level 2 System . . . 21
3.4.1 Front End Module L2 operation . . . 21
3.4.2 The L2 linker . . . 21
3.4.3 The L2 z-vertex determination . . . 21
3.4.4 The L2 fitter . . . 21
3.4.5 The L2 decider . . . 22
3.5 The level 3 system . . . 22

4 A level 1 z-vertex trigger for the FTT **25**
4.1 Motivation . . . 25
4.1.1 Sources of background . . . 25
4.1.2 Using a z-vertex to detect background . . . 25
4.2 Algorithm . . . 26
4.2.1 Overview . . . 26
4.2.2 Step 1: Reading the z information . . . 26

4.2.3 Step 2: Searching segments . . . 29
4.2.4 Step 3: Implementing a p_T-cut . . . 29
4.2.5 Step 4: Searching for tracks . . . 30
4.2.6 Step 5: Towards a trigger decision . . . 31
4.2.7 The 'Segment Slope' algorithm . . . 34
4.3 Hardware design . . . 34
4.4 Simulation . . . 35
4.5 Performance . . . 36
4.5.1 Input . . . 36
4.5.2 Segment finding . . . 36
4.5.3 Track resolution . . . 38
4.5.4 Vertex resolution . . . 38
4.5.5 Trigger concept . . . 39
4.5.6 The 'Segment slope' algorithm . . . 43
4.6 Summary . . . 44

5 A fast and accurate z-vertex determination for the level 2 FTT 49
5.1 Motivation . . . 49
5.2 Algorithm . . . 49
5.2.1 Overview . . . 49
5.2.2 z-outlier rejection . . . 51
5.2.3 Track fit . . . 51
5.2.4 Excluding tracks not originating from the primary vertex . . . 53
5.2.5 Calculating an accurate vertex position . . . 53
5.3 Hardware implementation . . . 53
5.4 Simulation . . . 54
5.5 Performance . . . 54
5.5.1 Outlier rejection . . . 54
5.5.2 Track fit . . . 55
5.5.3 Excluding tracks not originating from the primary vertex . . . 56
5.5.4 Calculating an accurate vertex position . . . 57
5.6 Summary . . . 57

6 Conclusions 59
6.1 The L1 FTT z-vertex trigger . . . 59
6.2 A refined z-vertex position for the L2 FT . . . 60

7 Acknowlegdments 61

Chapter 1

Introduction: Aim of this work

1.1 A level 1 z-vertex trigger

After a luminosity upgrade of the HERA accelerator, the trigger (event selection and filtering) of the H1 experiment has to cope with both higher signal and background rates. A powerful tool to distinguish electron/positron-proton interactions from various kinds of background is the position of the z-vertex, i.e. the position of the common origin of charged particle tracks along the beamline (see figure 1.1). The first goal of this diploma thesis was to establish if it is possible to determine the z-vertex using signals from the central drift chamber in H1 within the first level trigger latency of $2.2\,\mu$s. If so, an algorithm was to be developed to form a trigger decision based on this information, making as much use as possible of the new Fast Track Trigger (FTT). The functionality of the algorithm was to be tested with a simulation, whereby efficiencies and background rejection power were to be determined.

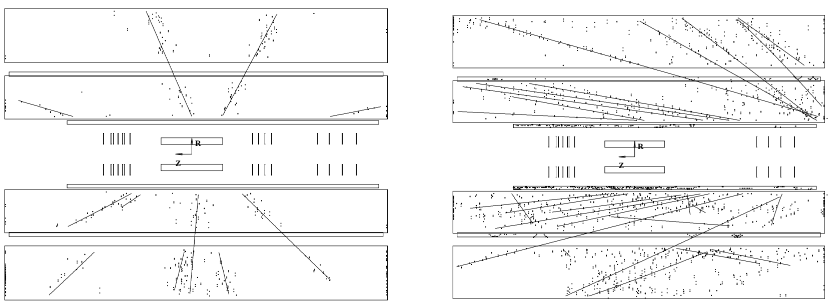

Figure 1.1: The figures show a side view of the H1 central tracking detectors. On the left, a signal event (open charm production in DIS) with tracks originating from the nominal interaction region is shown, whereas on the right, a typical background event (proton-collimator interaction) with tracks originating from the right is displayed. The lines correspond to reconstructed tracks, while the dots are the actual hits in the drift chambers.

1.2 A refined z-vertex determination for the Level 2 FTT

On the second trigger level, where a decision time of $20\,\mu$s is available, the Fast Track Trigger performs a vertex constrained track fit, i.e. determines detailed track parameters with an assumption about the track origin. The second part of this thesis is again concerned with a determination of the z-vertex position, but this time using refined track information from the FTT instead of more or less raw drift chamber signals. The goal was to find a fast algorithm (taking at most a few μs) reaching a high accuracy (resolution) in z to provide a useful input for the fit.

Chapter 2

H1 at HERA

2.1 The HERA storage ring

The HERA (*Hadron Electron Ring Anlage*) collider at DESY incorporates two accelerators in a common ring tunnel of 6.3 km length (figure 2.1). One accelerates protons counterclockwise to an energy of up to 920 GeV, the other boosts electrons or positrons clockwise to an energy of 27.5 GeV. The two beams are brought into collision inside the detectors H1 and ZEUS. Also part of HERA are the spin physics experiment HERMES, which directs the electron/positron beam onto a polarised hydrogen or deuterium target and the b-physics experiment HERA-B, where the interactions of the proton beam with a metal wire are studied.

Both the electron/positron and the proton beam consist of 180 packages (*bunches*) containing of the order of 10^{10} particles each. Whilst the electron bunches are relatively short ($\approx$ 8 mm), the proton bunches extend over $\approx$ 300 mm. Width and height of the beams within the experiments are well below one mm. Every 96 ns two bunches intersect inside the detectors, defining the *HERA-Clock* with a frequency of 10.4 MHz.

2.2 The HERA II luminosity upgrade

HERA is in operation since 1992, but has undergone an extended shutdown and upgrade [2, 3] in 2001, adding superconducting focusing magnets within H1 and ZEUS to increase the luminosity seen by the experiments. The newly introduced bending of the electron/positron beam close to the interaction point produces copious amounts of synchrotron radiation, which necessitated a new, elliptical beam pipe and radiation masks within the experiment. The proton machine underwent changes as well, necessitating new collimators within the experiments. At the time of writing, HERA II was being commissioned, and the synchrotron radiation induced background as well as the background caused by proton-collimator interactions proved to be a larger problem than expected, in part motivating this diploma thesis work.

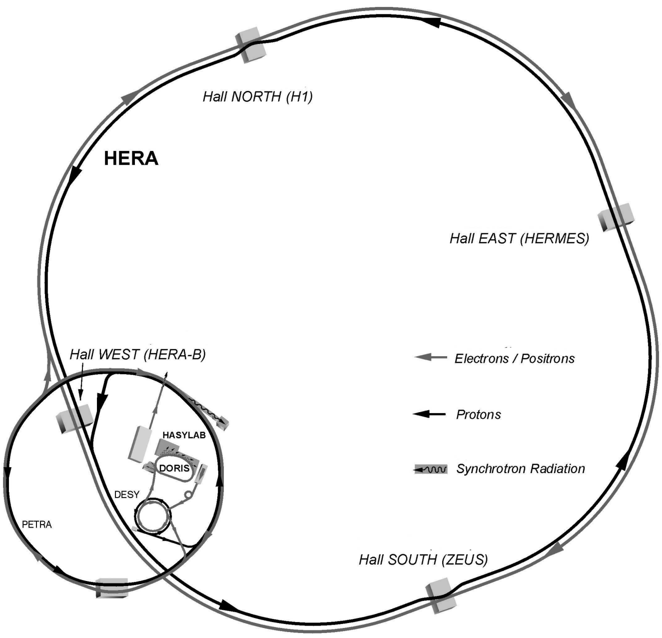

Figure 2.1: The accelerators at DESY (adapted from [1]).

HERA II	e-beam	p-beam
Energy	27.5 GeV	920 GeV
Number of bunches total/colliding	180/174	180/174
Particles per bunch	$4.2 \cdot 10^{10}$	$10 \cdot 10^{10}$
Beam current	58 mA	140 mA
Beam size $\sigma_x \times \sigma_y$	$118\,\mu\text{m} \times 32\,\mu\text{m}$	$118\,\mu\text{m} \times 32\,\mu\text{m}$
Luminosity	$7.36 \cdot 10^{31}\text{cm}^{-2}\text{s}^{-1}$	
Specific luminosity	$1.64 \cdot 10^{30}\text{cm}^{-2}\text{s}^{-1}\text{mA}^{-2}$	

Table 2.1: Design parameters of HERA II (from [2]).

2.3 The H1 detector

2.3.1 Overview

The H1 detector [4, 5] is located in the north of the HERA ring; the very complex apparatus was built and is maintained by a collaboration of about 400 physicists from 39 institutes located in 12 countries.

The experiment consists of three main sections, namely tracking, calorimetry and the muon system (see figure 2.2), each of which is made up of several subdetectors. The *tracking* detectors are located closest to the interaction point and measure tracks of charged particles. There are precision silicon detectors to identify decay vertices from long lived particles, multiple wire proportional chambers mainly used for triggering and drift chambers for the reconstruction of tracks. For the Fast Track Trigger and consequently also for this work, information from the central jet chamber (CJC) is used. It is described in more detail in section 3.2. The tracking detectors are surrounded by *calorimeters* which measure particle energies. In the forward[1] and central part a liquid argon detector with lead (electromagnetic part) and steel (hadronic part) absorber plates is used, whilst the backward spaghetti calorimeter identifies the scattered electron with a lead-scintillator-fibre detector. The tracking and calorimetry detectors are enclosed by a superconducting magnet, generating a field of 1.15 Tesla. Muons and high energy hadrons which pass the calorimeters are detected with streamer tubes installed between the iron plates of the magnet yoke and a separate *muon system* in the forward direction.

2.3.2 Trigger

A priori every HERA bunch crossing could produce *ep* (electron/positron - proton) interactions, corresponding to a rate of 10.4 MHz. The true *ep* rate is about 1 kHz, the background rate 10 to 100 times higher. However, only five to ten events per second can be written to tape; a reduction by a factor of about a million from the a priori rate and a factor of several hundred for *ep* events is needed. This is done by the trigger, which consists of 4 levels, designed to recognise interesting physics events and separate them from background.

Level 1

The first trigger level at H1 works dead-time free, i.e. the subdetectors continue writing data into their pipelines whilst fast algorithms process signals of a specific subdetector. The results are combined by the central trigger logic (CTL) to decide if the event deserves further consideration. If this is the case, the `L1 Keep` signal is issued 2.3 μs after the bunch crossing of interest and the pipelines are stopped, no further data are taken, i.e. *dead-time* starts.

Level 2

On the second trigger level, the decision of level 1 is refined by more involved trigger hardware; combined information from different subdetectors is used to calculate topological quantities and to feed a neural network. Within 20 μs after the `L1 Keep` either a `L2 Reject` or a `L2 Keep` are issued, whereupon either the pipelines are cleared and data taking restarts or the readout of the complete detector is initiated.

[1] The H1 coordinate system is based on the proton beam direction, which defines the z-Axis and the "forward" or "downstream" direction (see figure 2.2).

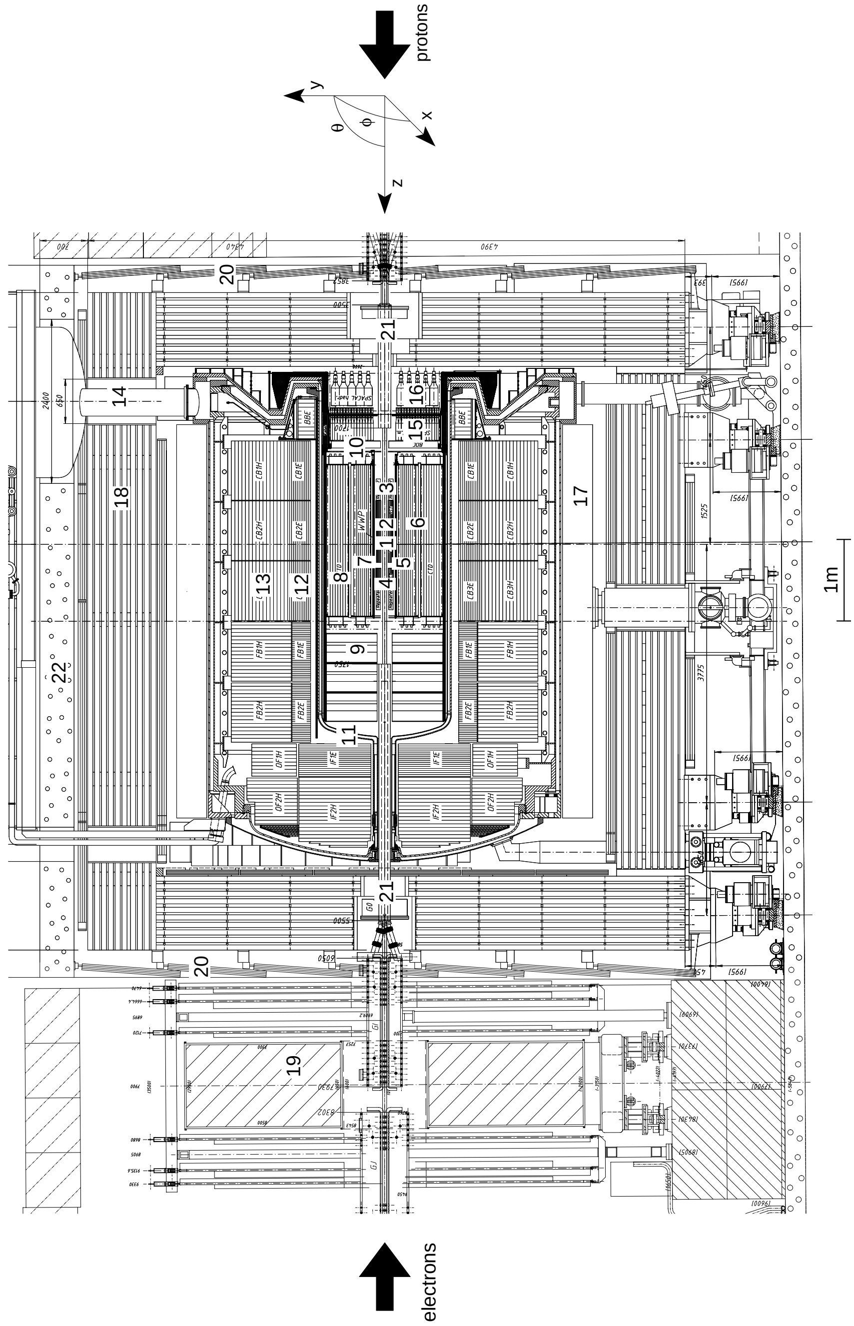

Figure 2.2: A cut through the H1 detector as it appears after the luminosity upgrade; see table 2.2 for the different subdetectors. The coordinate system used in H1 is shown on top.

	Detector component	Abbreviation
1	Nominal interaction point	IP
	Tracking detectors	
2	Central silicon tracker	CST
3	Backward silicon tracker	BST
4	Forward silicon tracker	FST
5	Central inner proportional chamber	CIP
6	Central outer proportional chamber	COP
7	Inner central jet chamber	CJC1
8	Outer central jet chamber	CJC2
9	Forward tracking detectors	FTD
10	Backward proportional chamber	BPC
	Calorimeters	
11	Liquid argon container	
12	Liquid argon electromagnetic calorimeter	LAr elm.
13	Liquid argon hadronic calorimeter	LAr hadr.
14	Liquid argon cryogenics system	
15	Electromagnetic spaghetti calorimeter	SpaCal elm.
16	Hadronic spaghetti calorimeter	SpaCal hadr.
17	Superconducting solenoid	
	Muon detectors	
18	Instrumented iron (central muon / tail catcher)	CMD/TC
19	Forward muon detector (incl. toroid magnet)	FMD
20	Veto wall / time of flight system	ToF
21	New superconducting focusing magnets	GO/GG
22	Concrete shielding	

Table 2.2: The main components of the H1 detector - legend to figure 2.2.

Level 3

The third trigger level is intended to abort the readout if detailed processing, now with software running on conventional processors, shows that the event in question is not worthy of further consideration. During the HERA I running period there was no level 3 system in operation, and only with the commissioning of the Fast Track Trigger described in the next chapter, a farm of L3 PowerPCs will be installed and issue `L3 Keep` and `L3 Reject` within about $100\,\mu$s of the bunch crossing of interest. Only with an `L3 Keep`, the detector readout is completed, which takes about 1 ms and should therefore occur less than 50 times per second to keep the primary dead-time below 5-10%.

Level 4/5

The forth and fifth level of the H1 trigger run on a farm of standard PCs. Two separate systems in the early years of H1 operation have been merged to a single one in 2002. It performs a full reconstruction of events, making use of the complete detector information. This is then used for the final decision on whether to keep or reject the event. If the event is kept, a complete dataset of detector information (RAW data) as well as a compressed version, containing reconstructed quantities such as track parameters (DST) are written to storage tape, where they await analysis. The level 4/5 system also provides time dependent calibration constants such as beam position or drift velocities, which are saved on a database and also fed back into the reconstruction code.

Chapter 3

The Fast Track Trigger

3.1 Motivation

The upgrade to HERA II promises ep rates about five times higher than in the HERA I running period. The trigger and data acquisition system will also be strained by much higher background rates. The existing DCRΦ (Drift Chamber $r - \phi$, [6]) track trigger detects tracks with a transverse momentum p_{T} greater than 400 MeV. Since the commissioning of that trigger in 1992, a new generation of programmable logic chips has become available and so a new trigger system, the Fast Track Trigger (FTT) was proposed [7, 8]. It will do a precise reconstruction of tracks with transverse momenta as low as 100 MeV on L2 and will even be capable of performing invariant mass sums on L3, thus greatly increasing the statistics for exclusive final states, especially those containing heavy quarks. An overview of the system and its main components is given in figure 3.1.

3.2 The Central Jet Chamber

The first two levels of the FTT work exclusively with signals from the Central Jet Chamber (CJC). The CJC [5] is built of two drift chambers, the inner CJC1 ranging from 20.3 cm to 45.1 cm and the outer CJC2 from 53.0 cm to 84.4 cm (see figure 3.2). They are made up of 30 respectively 60 cells in ϕ and cover a z-range from -112.5 cm to 107.5 cm. The cells are tilted by about 30° such that in the presence of the magnetic field, the ionisation electrons drift approximately perpendicular to high momentum tracks. Also, most tracks will cross a sense wire plane at least once, allowing to measure the passing time of the particle with a σ of about 0.5 ns, consequently identifying the bunch crossing of origin. As it is a priori impossible to decide from which side the ionisation electrons reach the wires, there is a so called right-left ambiguity, adding a mirror image of every track to the reconstruction. The cell tilt and a vertex assumption or the use of both CJC rings can resolve this ambiguity with the help of the wire plane crossings.

The position of a hit is reconstructed from the timing (t) and the pulse-integral (Q) in the Qt-analysis, with a single hit resolution of 140 μm in $x - y$ and 6 to 10 cm in z.

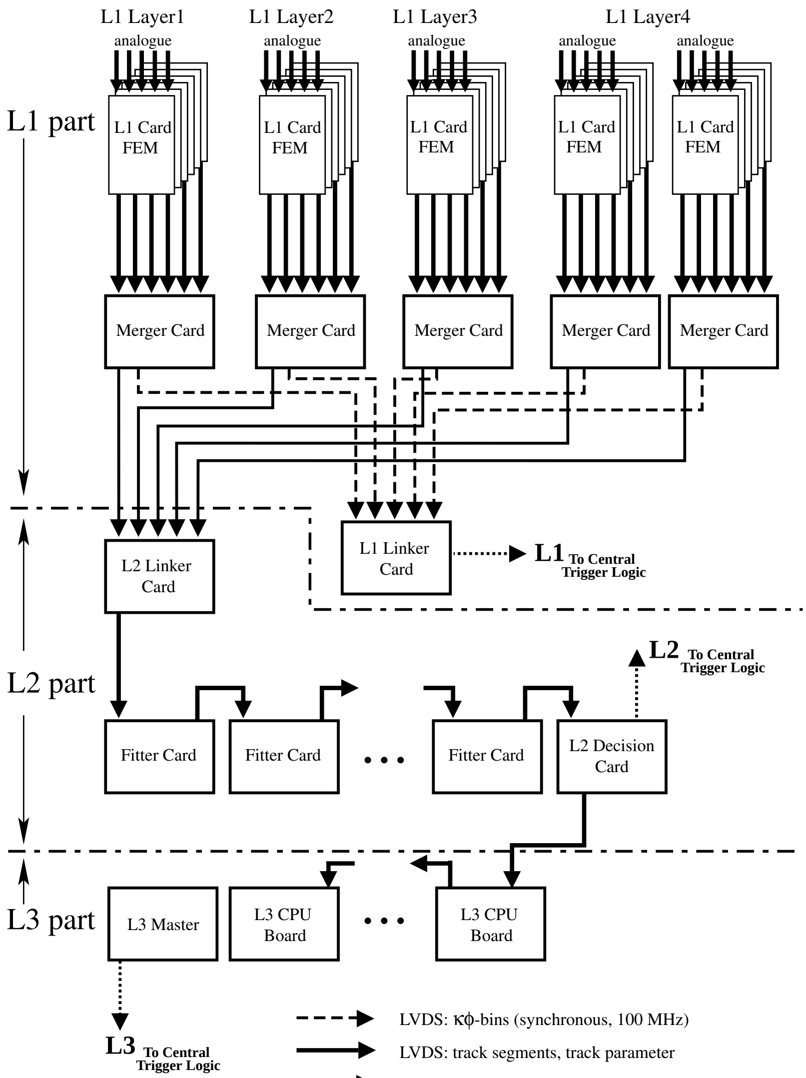

Figure 3.1: Block diagram of the main FTT components.

3.3 The level 1 system

3.3.1 Digitisation

The Fast Track Trigger [9, 10] is based on the signals of selected wires of the CJC. Three groups of three wires each are used in every cell of the CJC1 and one more group of three wires in the CJC2, giving 150 groups and 450 wires in total (see figure 3.2). A group of three wires at a fixed distance from the beam line is called a *trigger layer*, in which track segments will be identified. The signals from both ends of these wires

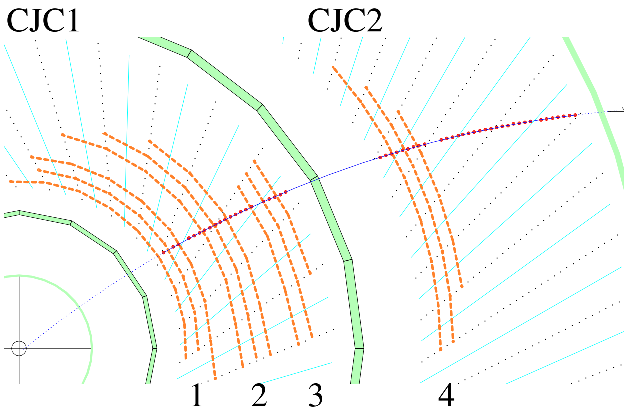

Figure 3.2: A cut through the Central Jet Chambers perpendicular to the beam line (located in the lower left corner), showing the twelve wire layers combining to the four trigger layers used for the FTT.

are tapped by analogue buffer cards[1], located on the FADC (*F*lash *A*nalogue - *D*igital *C*onverter) cards used for the standard digitisation of the CJC hits. The analogue cards drive the signals to the 30 Front End Modules (FEMs - see figure 3.3 for an overview of the design)[2]. On every FEM the signals from five trigger groups adjacent in ϕ are digitised using dual 10-bit linear ADCs[3] (*A*nalogue - *D*igital *C*onverters) operated at 80 MHz clock frequency[4]. The digitised data are then passed on to a farm of FPGAs[5], where the Qt analysis is performed. Its result is filled into shift registers synchronised at 20 MHz. The z information as well as the full 80 MHz time information is stored in additional 6 and 2 bit registers[6] respectively (see figure 3.4). The L1 FTT z-vertex trigger proposed in this thesis would get z information directly from the Qt analysis, as a different bit representation is required by transmission rate constraints.

---

[1]Designed and built by the University of Manchester.

[2]Built by Rutherford Appleton Laboratory (RAL), FPGA programming by RAL, the University of Birmingham and ETH Zürich.

[3]Analog Devices AD9218.

[4]All clock frequencies used for the FTT are multiples of the HERA Clock (10.4 MHz). Usually one talks 20, 80 and 100 MHz when meaning 20.8, 83.2 and 104 MHz respectively.

[5]Field Programmable Gate Arrays: High density programmable logic. For the FTT, chips of the Altera APEX20KE [11] family are used.

[6]A double pulse rejection ensures that only one hit can be registered within a 20 MHz time slice, thus allowing to encode the full timing information in 2 bits. The 6 bits in z correspond to bins of 3.4 cm, smaller than the intrinsic z resolution of the CJC even for highly ionising particles.

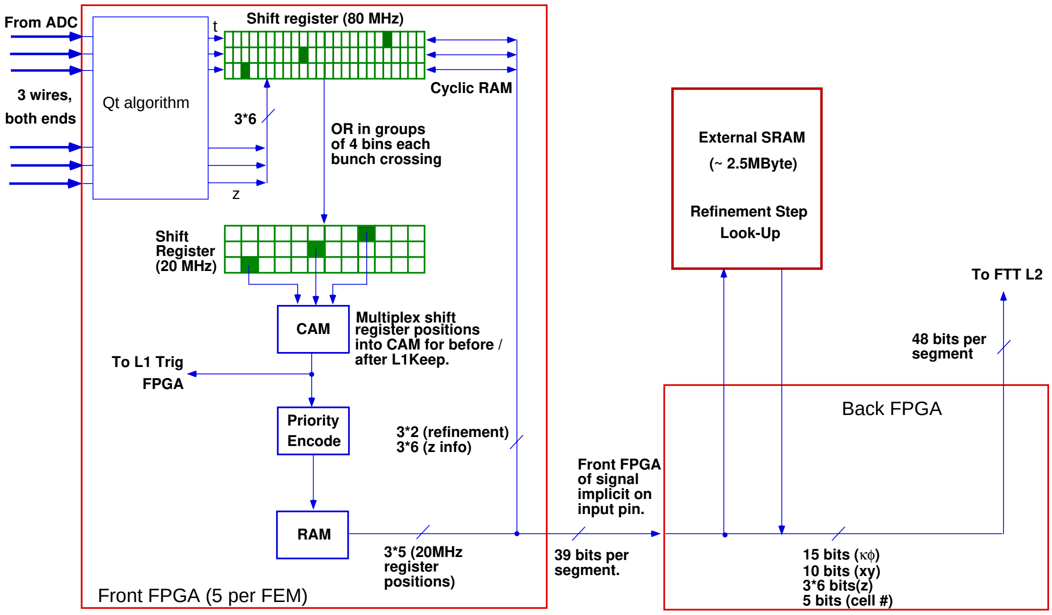

Figure 3.3: Functional layout of the Front End Module. There are 30 modules in total, each with five 'Front FPGAs' and one 'Back FPGA'.

3.3.2 Track segment finding

The information of the three shift registers in a cell plus one register from each of the neighbouring cells (see figure 3.5 and for the geometry of the corresponding wires figure 4.2) are searched for track segments. This is done by comparing the patterns in the shift registers with 3072 masks per cell, stored in so called Content Addressable Memories (CAMs - inverse RAMs, where the input is compared to the content (pattern) and the output is the memory address of the pattern location). The number of masks is sufficient to identify all possible segments of tracks with a p_{T} of more than 100 MeV and as the FPGAs are more than fast enough to perform a match every bunch crossing, all possible hit combinations for all possible t_0 hypotheses are considered.

For each track segment found in the CAMs, the corresponding κ (track curvature) and ϕ (track angle measured at the track apex) values are looked up and entered into a histogram for every cell. These histograms are then sent from the FEMs via merger cards to the L1 Linker card[7].

[7]Both merger and linker cards are FTT Multi Purpose Boards (MPBs) designed and manufactured by Supercomputing Systems (SCS), Zürich in close collaboration with ETH (see [12, 13, 14] for details on the hardware).

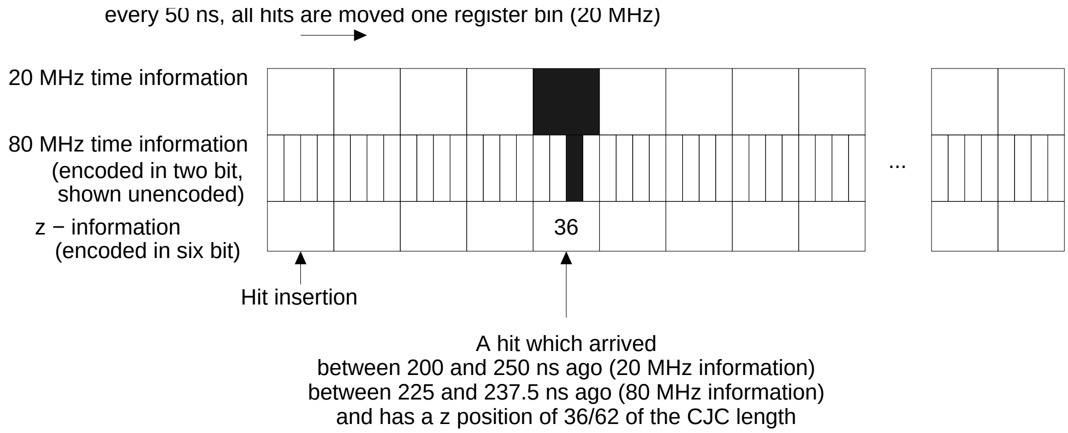

Figure 3.4: For every wire, a shift register as depicted stores 20 MHz and 80 MHz time information as well as the z-position for every hit.

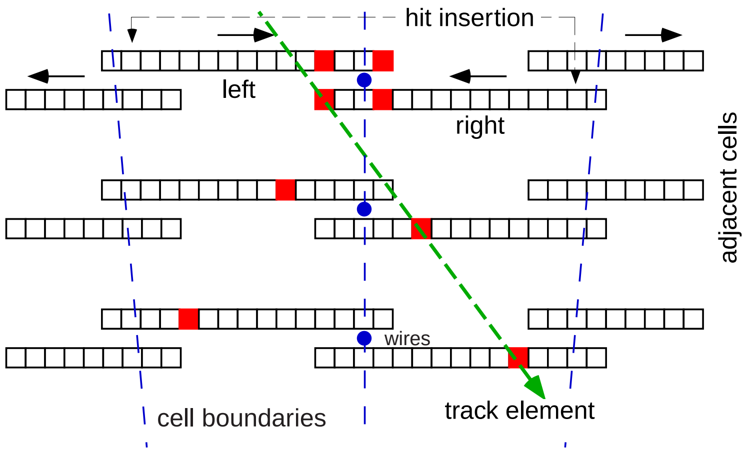

Figure 3.5: The shift register technique used to identify track segments on L1

.

3.3.3 Track segment linking

On the linker card, the cell wise histograms are combined to one global 8×60 histogram in the $\kappa - \phi$ plane for every trigger layer. Track segments with compatible κ and ϕ values are then searched for, using a 3×3 sliding window on the four histograms. If at least two segments on different trigger layers match, a track is flagged. Even tough individual track segments can fit into the masks for several bunch crossings, a successful link is usually only possible if the t_0 hypothesis is correct, thus defining the FTT t_0 as the bunch crossing, where the linking quality of all track candidates reaches a maximum.

The FTT L1 system generates up to 32 trigger elements, 16 of which (see table 3.1) are foreseen to be selected and made available to the central trigger logic. The FTT trigger elements can easily be adapted to new physics needs by simply reprogramming an FPGA.

TE	*condition*
0	any track (event t_0)
1 2 3	number of tracks (0-7) with $p_{\mathrm{T}} > 100\,\mathrm{MeV}$
4 5	number of tracks (0-3) with $p_{\mathrm{T}} > 125\,\mathrm{MeV}$
6 7	number of tracks (0-3) with $p_{\mathrm{T}} > 167\,\mathrm{MeV}$
8 9	number of tracks (0-3) with $p_{\mathrm{T}} > 250\,\mathrm{MeV}$
10 11	number of tracks (0-3) with $p_{\mathrm{T}} > 400\,\mathrm{MeV}$
12 13	number of tracks (0-3) with $p_{\mathrm{T}} > 600\,\mathrm{MeV}$
14 15	number of tracks (0-3) with $p_{\mathrm{T}} > 909\,\mathrm{MeV}$
16 17	number of tracks (0-3) with $p_{\mathrm{T}} > 1810\,\mathrm{MeV}$
19 20 21	charge Q_{tot} encoded
22 23 24	three different back-to-back topologies
25 26	two different jet topologies
27 28	$\sum E_T$ thresholds
29 30	$\sum p_T$ thresholds
31	$v_{antiparallel}$ threshold

Table 3.1: The proposed set of level 1 trigger elements (TEs).

3.4 The level 2 System

3.4.1 Front End Module L2 operation

If the central trigger takes a positive L1 decision, the `L1Keep` signal reaches the FTT a fixed $2.4\,\mu$s after the bunch crossing of origin. All pipelines and shift registers are stopped and the shift register - CAM match of level 1 is repeated, using bins shifted by the appropriate time delay.

The output addresses of the CAMs are then encoded and written to a FIFO (First In, First Out) buffer. At the same time, a lookup is performed to identify the original hits activating a CAM match in order to retrieve the refined t and the z information from the parallel shift registers. It is then checked further whether the segment can still belong to a track originating from the vertex region, taking into account the full t information. The refined masks used for this step are strongly dependent on calibration constants such as drift velocity and beam position and will therefore be updated regularly. For those segments, that are fitting the masks, the curvature κ, the slope ϕ and the precise coordinates of the central hit in x and y are looked up in a RAM and the z coordinates of all three hits are retrieved from the shift registers and sent together to the L2 system.

3.4.2 The L2 linker

The L2 system uses the same set of merger cards as the L1 system, but after `L1Keep`, the segment information is forwarded to the L2 linker card, where again the segments are combined to tracks, this time using a set of four histograms with 40×640 bins in the κ–ϕ plane each. A 3×3 bin sliding window is applied on sub-arrays of the full histogram using CAMs and searches for links. As soon as a track was found (i.e. at least two segments lie close enough in κ–ϕ space), the relevant information is sent to one of the six fitter cards.

3.4.3 The L2 z-vertex determination

The Level 2 z-vertex algorithm proposed in this thesis uses the z-information of the linked segments of the first 24 tracks to calculate the vertex position in z. It would reside in the data controller FPGA of the first fitter card. The z-vertex position is then used as a constraint to the $r-z$ fitting step described below.

3.4.4 The L2 fitter

Each fitter card is equipped with four floating point digital signal processors (DSPs), where every track is first fitted to a circular trajectory originating from the primary vertex using the non-iterative method of V. Karimäki [15] in the $r-\phi$ plane. In a second step, a fit in the $r-z$ plane is performed using a vertex constraint either from the CIP z-vertex trigger or the algorithm proposed in this thesis. The four DSPs per card can perform two fits each within the L2 latency, allowing for 48 tracks to be fitted on the six cards. The results of the fits are then passed on to the L2 decider card.

3.4.5 The L2 decider

On the L2 decider card, track based event quantities such as momentum sums are used to generate the L2 trigger elements (see table 3.2). In addition, the L1 trigger decision can be verified using the more precise information available on L2.

3.5 The level 3 system

A farm of up to 16 commercial VME PowerPC boards uses the information of the FTT L2 system to search for particle resonances. Also first level trigger information from other subdetectors is included for particle or jet identification already at trigger level. A real time operating system allows to run event analysis code provided by physics working groups to refine the trigger decision and improve signal over background ratios for the triggered events.

TE	*condition*
0 1 2	number of tracks (0-7) with $p_{\mathrm{T}} > 100\,\mathrm{MeV}$
3 4	number of tracks (0-3) with $p_{\mathrm{T}} > 200\,\mathrm{MeV}$
5 6	number of tracks (0-3) with $p_{\mathrm{T}} > 400\,\mathrm{MeV}$
7 8	number of tracks (0-3) with $p_{\mathrm{T}} > 1\,\mathrm{GeV}$
9 10	number of tracks (0-3) with $p_{\mathrm{T}} > 2\,\mathrm{GeV}$
11 12	number of tracks (0-3) with $p_{\mathrm{T}} > 5\,\mathrm{GeV}$
13 14 15	charge Q_{tot} encoded
16 17 18	three different back-to-back topologies
19 20 21 22	several different jet topologies
23	single hemisphere topology
24 25	$\sum E_T$ thresholds
26 27	$\sum p_T$ thresholds
28	$v_{antiparallel}$ threshold
29	$\|z_{vtx}\| < 50\,\mathrm{cm}$ (new)
30 31 32 33	elastic ρ elastic ϕ elastic J/Ψ elastic Υ

Table 3.2: A possible set of level 2 trigger elements; they partly validate the L1 elements, and partly deliver new information. As these trigger elements are still under study, they are subject to change in the final implementation.

Chapter 4

A level 1 z-vertex trigger for the FTT

4.1 Motivation

4.1.1 Sources of background

At a much higher rate than ep-interactions occur, so called background events take place. There is a wide variety of sources for these, namely interactions of one of the beams with the rest gas in the beam pipe (*beam-gas*), interactions of stray beam particles with the beam pipe (*beam-wall*) and with collimators, and synchrotron radiation conversion in any part of the detector. The increase in synchrotron radiation and a new collimator installed at $z = -80\,\mathrm{cm}$ lead to a significant increase of background rates after the upgrade to HERA II.

4.1.2 Using a z-vertex to detect background

The position of the common origin of tracks along the z-axis is a very powerful tool to discriminate background from genuine ep interactions. Due to the short length of the particle bunches, ep events only occur in a narrow region around the nominal interaction point, whereas beam-gas events occur with equal probability at any point along the beam line and interactions with collimators obviously produce tracks originating from the location of the collimator. A system which is able to reconstruct the z-vertex on trigger level 1 is therefore a very efficient way to reject events not originating from the signal region. At H1, a z-vertex trigger based on two multiple wire proportional chambers (MWPC), the CIP and COP (Central Inner/Outer Proportional chamber), radially located just inside and just outside the CJC1 respectively was in operation for the past running periods. For the HERA II luminosity upgrade, also a new z-vertex trigger was installed, based on an improved five layer CIP alone, leading to a higher angular acceptance. At the time of writing, this system, the CIP2000 and the corresponding trigger, were in the commissioning phase and it was recognised that due to temperature problems at most three of the five layers could be operated simultaneously. As some sort of z-vertex trigger is essential for recognising genuine *ep* interactions, a certain redundancy is desirable. One of the goals of this diploma thesis was to investigate, whether and how a z-vertex trigger could be implemented within the framework of the FTT, thus relying on a existing and well understood subdetector, the CJC, and reducing the need for new hardware to a minimum[1].

4.2 Algorithm

4.2.1 Overview

The FTT z-vertex trigger algorithm performs five main steps: first, the results of the Qt-algorithm are projected onto the $r-z$ plane for every cell of the CJC. In every CJC1 trigger layer (three wires in every cell of the CJC1 at a fixed r, see figure 3.2), hit patterns corresponding to $r-z$ track segments are identified in a second step. In the third step, the results of the first few steps of the $r-\phi$ algorithm are used to check whether the cell and layer containing the $r-z$ segment also contains an $r-\phi$ segment of a minimum transverse momentum. The fourth step combines the information from several cells to form ten sectors in ϕ. In each of these sectors, all possible combinations of segments to tracks produce an entry in the *intersect histogram*, corresponding to the intersect of the track with the z-axis. The fifth step combines the 10 intersect histograms to a final *vertex histogram*, which is then searched for peaks to identify the position of the z-vertex. Figure 4.1 shows a flow diagram of the L1 algorithm, also indicating where in the hardware every step is performed.

4.2.2 Step 1: Reading the z information

The charge division algorithm performed in the Front End Module front-FPGA[2] returns a z value for every hit. The existing $r-\phi$ algorithm fills 6 bit encoded z-information into shift registers and searches for track segments (see section 3.3). The z information is then sent along with the track segment information to be used for 3-dimensional fitting on level 2.

The proposed algorithm sends the z-information of the group of three wires to the back FPGA of the FEM (this FPGA is up to now mainly used for sending data to the merger chain and therefore has ample space to house the L1 algorithm) and performs an un-encoding. The following steps are performed for each cell and trigger layer separately. The z values from the innermost wire of the left and the outermost wire of the right neighbouring cell are ORed with the respective wires in the cell concerned. This combination takes into account tracks which cross cell boundaries due to the tilted CJC wire planes and achieves a high acceptance (see figure 4.2). The tested implementation uses 48 bits

[1]Indeed, only a single additional multi purpose board and a few cables will be required to implement the proposed algorithm.

[2]The FEMs are equipped with six FPGAs, five 'front' ones where most of the L1 algorithm is performed and one back one for the communication with the rest of the FTT.

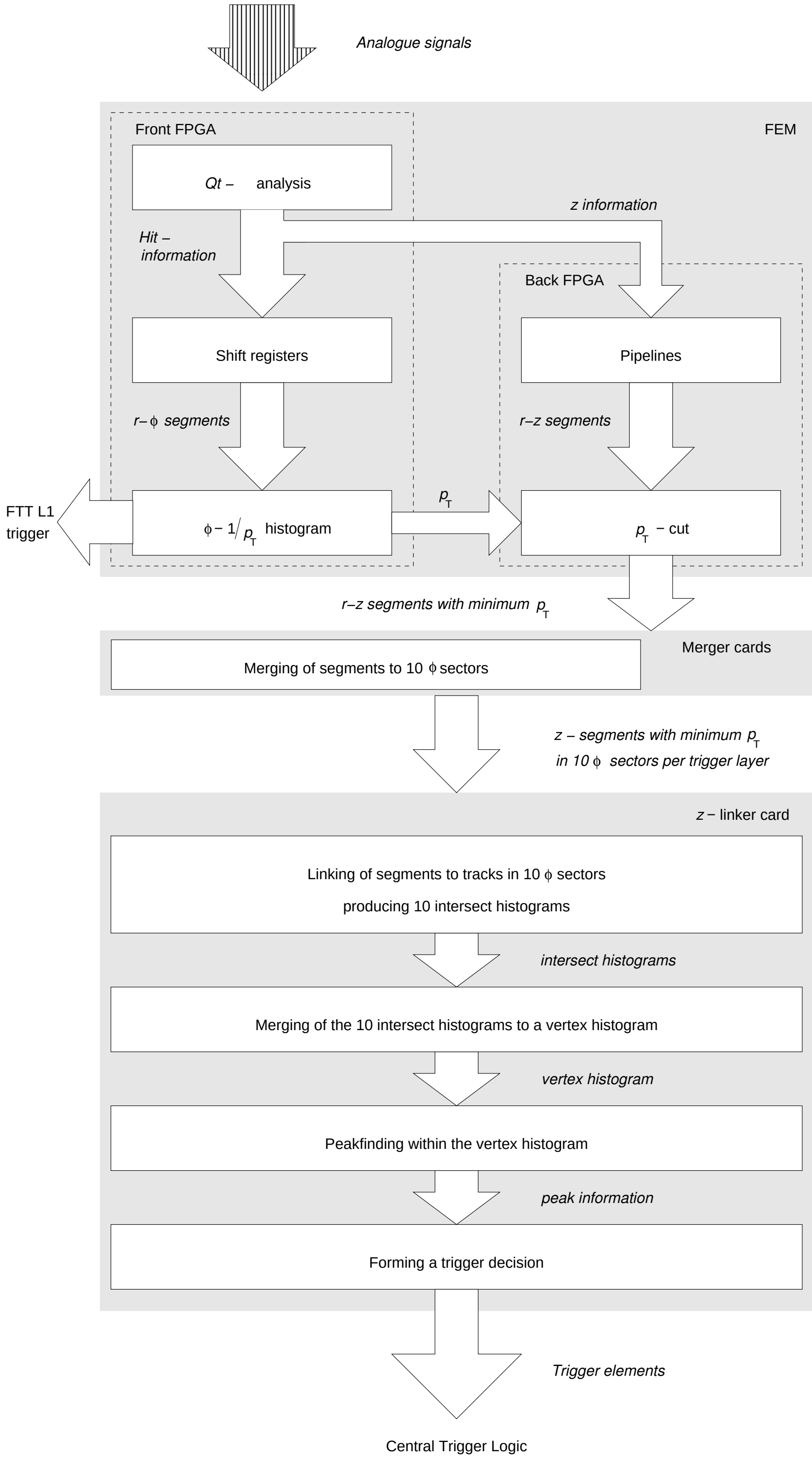

Figure 4.1: Overview of the L1 z-vertex trigger. All parts of the $r-\phi$ system not used are omitted.

unencoded z information[3]; values 0 and 47 are reserved, leaving 46 values to encode the position of the hit, each corresponding to a bin size of 4.8 cm[4].

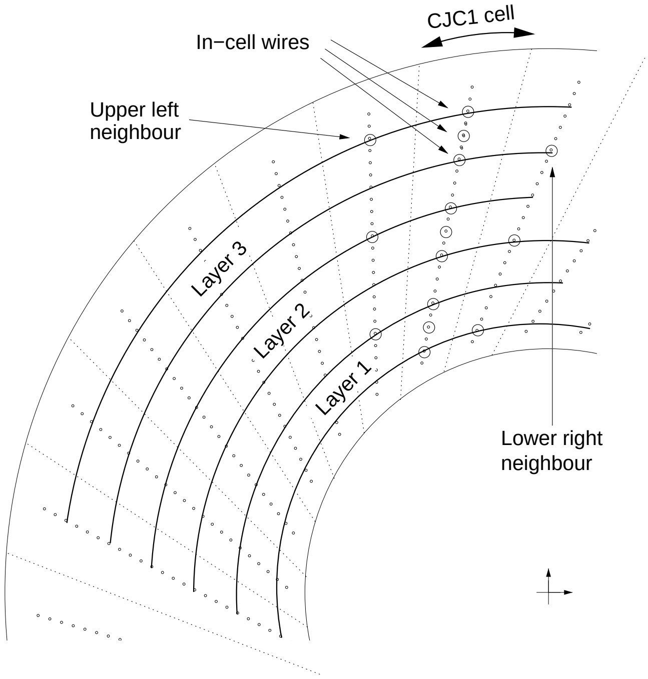

Figure 4.2: Geometry of the wires used for FTT in the inner central jet chamber CJC1.

It is a priori not known from which bunch crossing a drift chamber hit originates, as the drift can take up to 1.1 μs, corresponding to eleven bunch crossings. The presented algorithm does not try to identify the time where the interaction took place (t_0) as this is already done by the r–ϕ part of the FTT. Instead, the algorithm is repeated at the HERA frequency, making a new t_0 assumption every time. This is implemented as follows: For every possible z position on a wire, a 11 bin pipeline[5] is set up. At the same time as a hit is filled into the shift registers, it is also filled into the pipeline. Every bunch crossing, it is then moved by one bin and falls out of the pipeline after eleven bunch crossings, corresponding to the maximum drift time (see figure 4.3).

[3]The particular value of 48 is determined by transmission capacity constraints, see section 4.5.2 for details.

[4]This is still shorter than the intrinsic single hit z resolution of the CJC of 6 to 10 cm.

[5]A possible enhancement of the algorithm would be to introduce a layer dependent pipeline length corresponding to the respective maximum drift time.

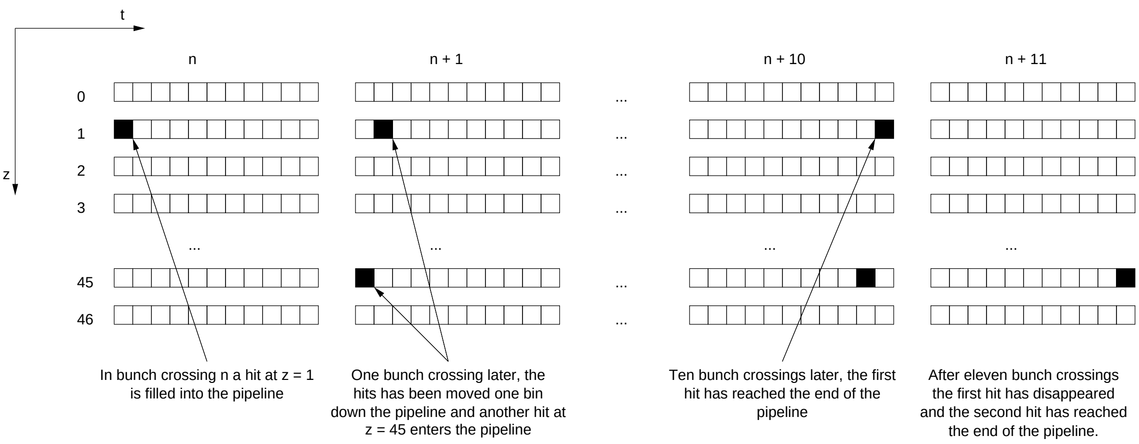

Figure 4.3: The pipelines used to account for drift times.

4.2.3 Step 2: Searching segments

Now, collecting the information from the three wires in a trigger layer (performing an OR over all bins of the pipeline for each wire), valid hit patterns are searched for (this is also where the 'Segment Slope' algorithm described later on (section 4.2.7) would come into play). If there is z information from at least two wires within a three bin window, a *track segment candidate* is flagged at the corresponding z position (see figure 4.4 and figure 4.9 for possible hit patterns).

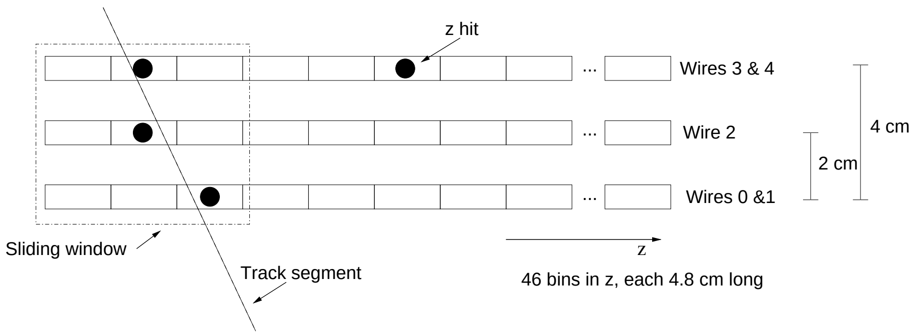

Figure 4.4: The sliding window used to search for valid z-hit patterns within a trigger layer

4.2.4 Step 3: Implementing a p_T-cut

Tracks originating from the interaction vertex will usually be reconstructed by the FTT with a higher transverse momentum (p_T) than tracks originating from interactions of the secondary particles with the beam pipe or parts of the detector (see figure 4.5). This is due to the fact that the track segment masks are generated using a vertex constraint; tracks not originating from the beamline are therefore usually reconstructed with a higher curvature corresponding to a lower p_{T}. The goal of a z-vertex trigger is to identify the

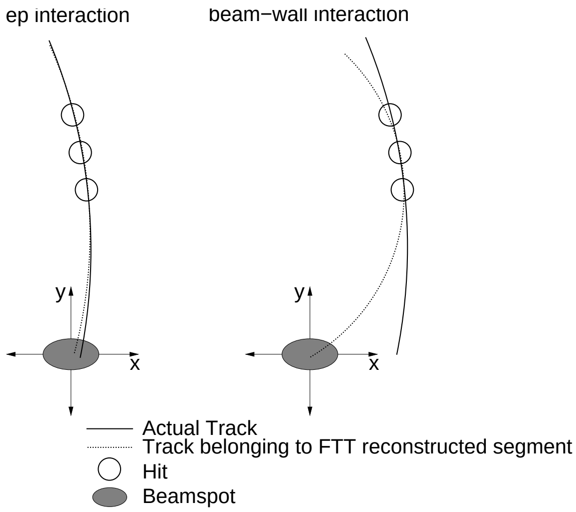

Figure 4.5: Tracks originating from the interaction vertex (left) will usually be reconstructed by the FTT with a higher transverse momentum (p_{T}) than tracks originating from interactions of the secondary particles with the beam pipe or parts of the detector (right). This is due to the fact that the track segment masks used assume that the track originates from the beamline. The figure is not drawn to scale.

position of the primary vertex and ignore any secondary vertices as good as possible. For the proposed algorithm it is easiest to use the information from the $r-\phi$ algorithm to implement a p_{T}-cut: For every track segment candidate found in step two, it is checked against the p_{T} information stored in the CAMs (see [10, 9]), if the $r-\phi$ segment finder algorithm has found at least one segment with a minimum transverse momentum in the corresponding cell. If so, the z information of the segment is sent via merger cards to a z linker card[6] where the following steps are performed. Otherwise the segment candidate is rejected and no further processing occurs.

4.2.5 Step 4: Searching for tracks

The core of the L1 z-vertex trigger is the step from segments to tracks, combining the information from different layers and cells. First, the CJC 1 is divided into ten sectors in ϕ, each completely covering an angle of 36° and having some overlap with neighbouring sectors on trigger layers 1 and 3 (see figure 4.6). In every sector, a 46 bin array is set up for the three trigger layers. The bins corresponding to the z position of track segments are activated. All combinations of track segments from two out of three trigger layers

[6]The only additional hardware needed is a multi-purpose-board for the z linker, see figure 4.10.

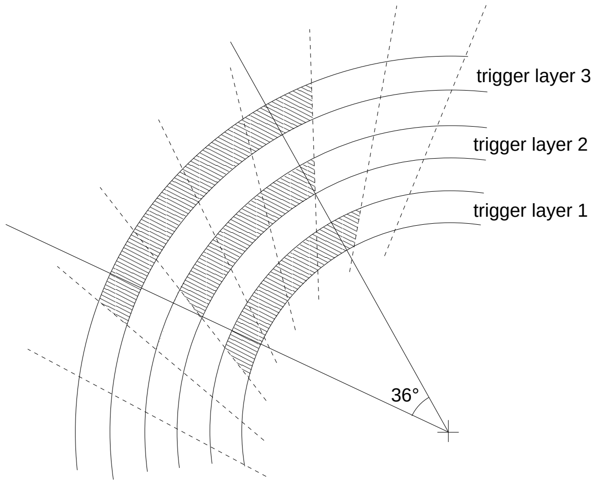

Figure 4.6: Coverage of one sector in ϕ.

are formed and fitted to a straight line which is extrapolated to the beam axis. The corresponding z-vertex is obtained by a look-up and added to a 40 bin *intersect histogram* (see figure 4.7), now representing a region of $z = -200\,\mathrm{cm}$ to $z = 200\,\mathrm{cm}$, giving a coarser bin size of 10 cm (for the geometrical acceptance of this algorithm, also in comparison to the CIP2000, see figure 4.8). The idea behind this is that the links between segments originating from the same track will point to the interaction vertex, leading to a crowding of histogram entries there, whereas the "wrong" links will produce a more or less evenly distributed 'combinatorial background'. This method is also used by the MWPC z-vertex trigger [4, 16, 17] and the CIP2000 z-vertex trigger [17, 18, 19, 20, 21], but with input from the CIP and the COP or the CIP alone respectively. It should be noted that the straight line assumption for the tracks is an approximation, as especially low momentum tracks are bent considerably in the magnetic field of the detector; tracks follow helix trajectories whose projection to the $r-z$ plane is a sine. It can be approximated by a straight line only if r is not too large and the track curvature κ is not too small. Studies have shown however, that the effect of bent tracks can be neglected in the z-vertex reconstruction (see section 5.2.3).

4.2.6 Step 5: Towards a trigger decision

In the next step the intersect histograms of the 10 ϕ-sectors are combined to a single *vertex histogram*. This is then analysed to form a trigger decision - several methods to do this are proposed. They are described below, the results of tests with H1 data can be found in section 4.5.5.

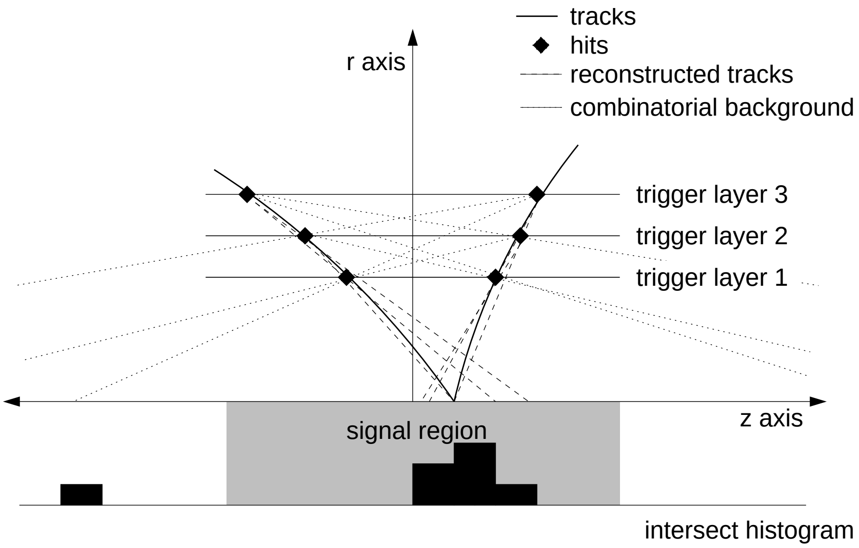

Figure 4.7: The algorithm used to find tracks in the $r-z$ plane (not to scale).

Method 1: 'Good Fraction'

The simplest method is to count the histogram entries within the signal region (here taken to reach from -60 cm to $+60$ cm) and compare this number to the entries outside the signal region. This is essentially the method used by the CIP2000 z-vertex trigger. In the case of the FTT z-vertex trigger, it does not appear to be particularly well suited, as it is unable to discriminate against the inevitable combinatorial background, which is confirmed by studies using data (see section 4.5.5).

Method 2: 'Top Peak'

All the following methods are based on a peak finding algorithm: First, yet another histogram containing a weighted sum of three adjacent bins of the vertex histogram is calculated. In this histogram then the peak search is performed. The 'Top Peak' method just identifies the highest peak and checks whether it is located within the signal region; if this is the case, the event is triggered. If two bins with the same number of entries form the peak, the backward one is selected.

Method 3: '$\frac{3}{4}$-Peak'

In the '$\frac{3}{4}$-Peak' decider method, also secondary peaks which reach at least three quarters of the height of the 'Top Peak' are taken into account. For a positive trigger decision it is required that a majority of these peaks is within the signal region, where the 'Top Peak' is weighted by a factor of 2.

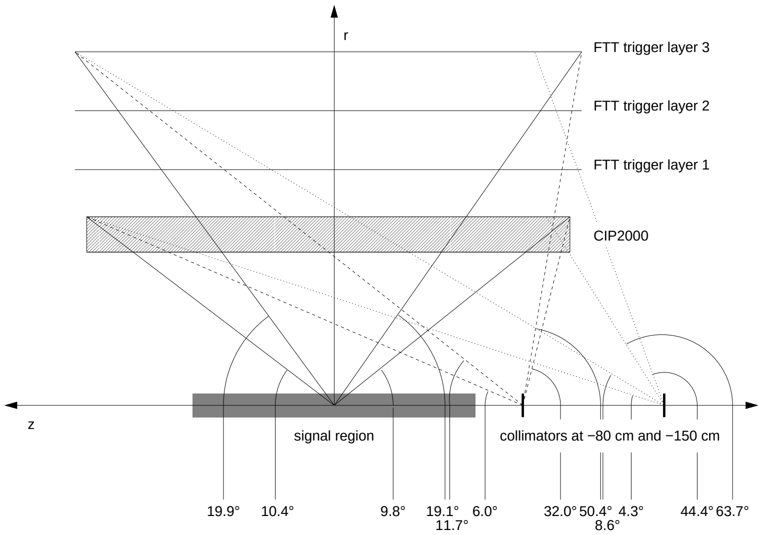

Figure 4.8: The geometrical acceptance of the FTT z-vertex trigger and the CIP2000. The minimum track angle with respect to the beam axis for a track to be visible to the two systems are indicated on the bottom for tracks originating from the nominal interaction point and the collimators at $z = -80\,\mathrm{cm}$ and $z = -150\,\mathrm{cm}$. The r axis is scaled by a factor of four compared to the z axis.

Trigger elements

A variety of other deciders were also considered but did only complicate the algorithm without increasing the efficiency or rejection power significantly. It is proposed to send up to eight trigger elements to the central trigger logic - a possible set of such elements is given in table 4.1.

TE	*condition*
0	At least two entries in the vertex histogram
1	Accept/veto of the $\frac{3}{4}$-Peak method
2	Top Peak within 60 cm of IP
3	Top Peak within 50 cm of IP
4	Top Peak within 40 cm of IP
5	
6	Significance of the Top Peak
7	

Table 4.1: A possible set of L1 z-vertex trigger elements.

4.2.7 The 'Segment Slope' algorithm

Complementary to the linking algorithm described above, the 'segment slope' algorithm tries to identify the slope of each individual track segment. Due to its larger geometrical acceptance this algorithm is therfore able to recognise background coming from beam-gas and beam-wall interactions in the far forward and the far backward region. It checks the pattern in the 3×3 sliding window used by the z-finder algorithm (4.2.2) against a table of all 512 possible hit combinations, where the 'slope' of the patterns is noted (see figure 4.9). If there is a minimum number of segments with identifiable slope in

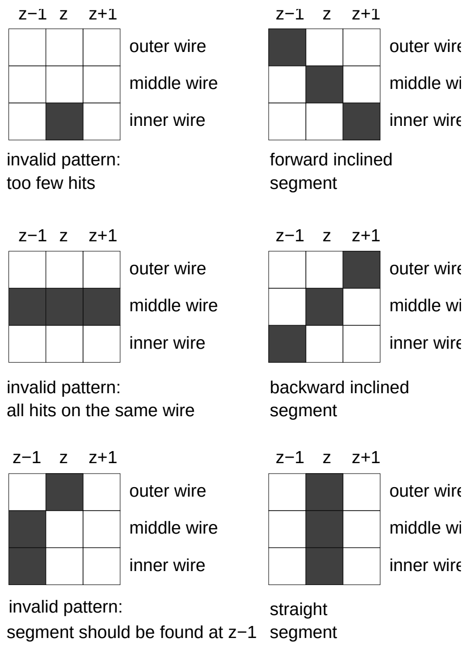

Figure 4.9: Examples from the classification according to segment slopes of hit patterns.

the upstream third of the CJC[7], the difference between forward and backward inclined segments is calculated. If a majority points away from the vertex, the event is rejected. This algorithm is only sensitive to high multiplicity, extremely forward or backward events. As it can be implemented with a very small additional effort (the pattern recognition has to be done anyway for finding segments), it was nonetheless studied.

4.3 Hardware design

The FTT z-vertex trigger was developed to make as much use as possible of the existing L1 FTT trigger design. The Qt algorithm performed in the front FPGA of the FEMs

[7]The downstream third is not considered as there is little background originating from the forward region

is tapped and only the last step has to be adjusted to account for the different binning. The pipelines and the z-segment finder can easily be fitted into the FEM back FPGA. The existing design of the merger cards has the capability of including a new component, an additional multi purpose board, the z linker (see figure 4.10 for an overview of the connections).

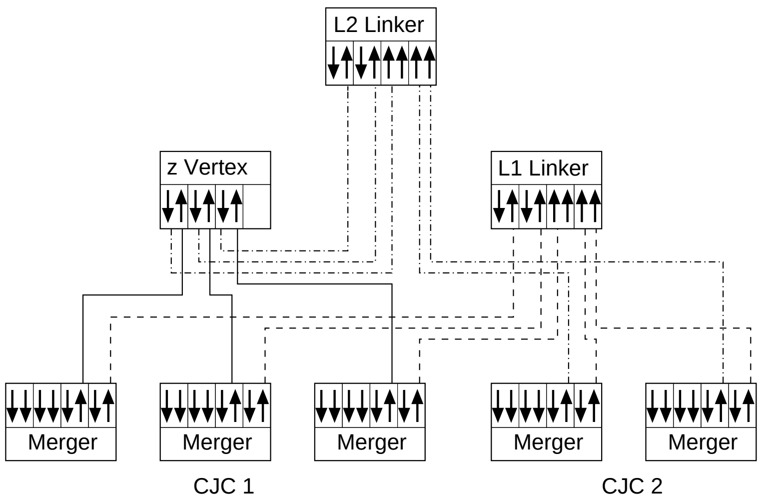

Figure 4.10: The merger chain, showing IO (input/output) and II (double input) cards (arrows) and the flow of data for the z-vertex trigger (solid lines), the L1 $r-\phi$ trigger (dashed) and the L2 mode (dot-dashed plus solid lines).

4.4 Simulation

To test the performance of the algorithms as described in the previous sections, they were simulated on a `Linux` PC. The official FTT simulation `FTTemu` in version 4.03 was modified to incorporate the different binning in z and used to emulate the hit finding and the charge division as well as the whole FTT $r-\phi$ algorithm. As input for `FTTemu`, Monte Carlo as well as data files were used. From the output a `ROOT`-tree [22] was filled using the FTT-`ROOT` interface `FTT++`. A script written in `C/C++` was then used to simulate the FTT z-vertex trigger. The results were analysed with the `ROOT` package. The use of a `ROOT` script for the simulation led to some performance losses, but allowed for easy debugging, fast adaption of parameters and provided a straightforward interface to the graphics and histogram facilities of `ROOT`.

4.5 Performance

4.5.1 Input

The performance of the L1 z-vertex algorithm was tested and tuned using a set of 1000 Monte Carlo events including a full simulation of the FTT hit digitisation and with several datasets where either the raw standard CJC hits or hits recalculated from the reconstructed tracks were used. The details of the samples can be found in table 4.2. The recreation of hits and the full hit digitisation simulation are not fully consistent; the number of segments found and the attainable resolution differ considerably for the two methods, but for the trigger efficiencies the difference is negligible.

Dataset	Physics	Cuts
Monte Carlo	AROMA 21 generated open charm in deep inelastic positron scattering	$0.5 < Q^2 < 200\,\mathrm{GeV}$ $0.1 < y < 0.9$
Background 96	L2 and L4 transparent run without ToF	any L1 trigger
Background 02	First collisions in 2002 running period, dominated by synchrotron radiation hits and beam-wall interactions	any L1 trigger
Positron 02	2002 positron only run	DCRΦ t_0
Proton 02	2002 proton only run	DCRΦ t_0
J/Ψ	Inclusive J/Ψ sample	μ pair compatible with J/Ψ
b-μ	μ plus jets	1 central μ, $p_\mathrm{T} > 2\,\mathrm{GeV}$ plus 2 jets with $E_T > 5\,\mathrm{GeV}$ each.
NC	Neutral current	$p_\mathrm{T}^{hadr} > 12\,\mathrm{GeV}$ $y < 0.9$

Table 4.2: Datasets used for performance tests and tuning

4.5.2 Segment finding

The binning of z-hits by the charge division algorithm is the first parameter which can be tuned to increase the efficiency of the FTT z-vertex trigger. An upper bound is put onto the number of bins by the restricted capacity of the link between the merger cards and the z-linker: On a 48 bit link running at 104 MHz, 480 bits can be sent per bunch crossing, resulting in again 48 bits for every sector in ϕ. 2 bits are foreseen for control, leaving at most 46 bits to represent the z coordinate. A finer binning has the advantage of a higher resolution, whereas with a coarser one, the physical size of the 3 bin sliding window increases and the segment finding efficiency rises. Figure 4.11 shows that the bin size dependence of the efficiency is rather small and it is advantageous to use the maximum possible number of bins. The scatter plots of figure 4.12 show that the z

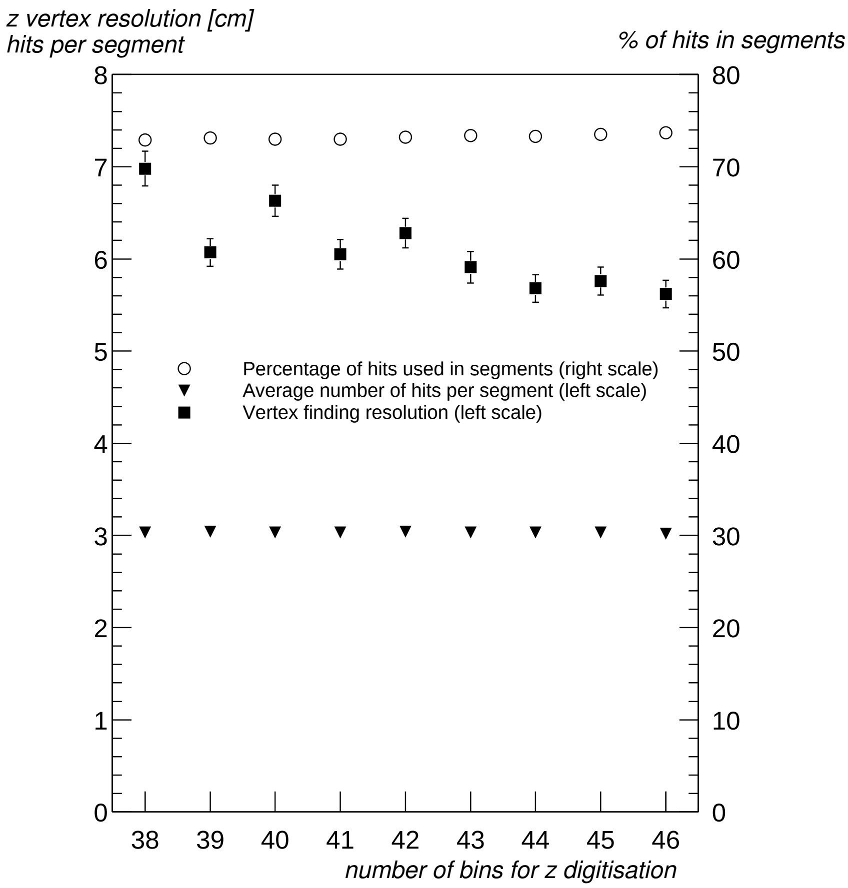

Figure 4.11: Efficiency and resolution of the segment finding algorithm versus number of bins in the charge division output. Plotted are the percentage of hits included in segments and the average number of hits per segment. The resolution was determined by running the full simulation and comparing the position of the Top Peak with the position of the offline reconstructed vertex. Plotted is the standard deviation of a Gaussian fit to the difference distribution. The errors are the uncertainties of the fit.

segment multiplicity is about a factor of two lower than the corresponding quantity in the $r-\phi$ algorithm, if the p_{T} cut is not too harsh. This is expected, as a particular hit combination can fire several $r-\phi$ masks but fits at most one $r-z$ pattern.

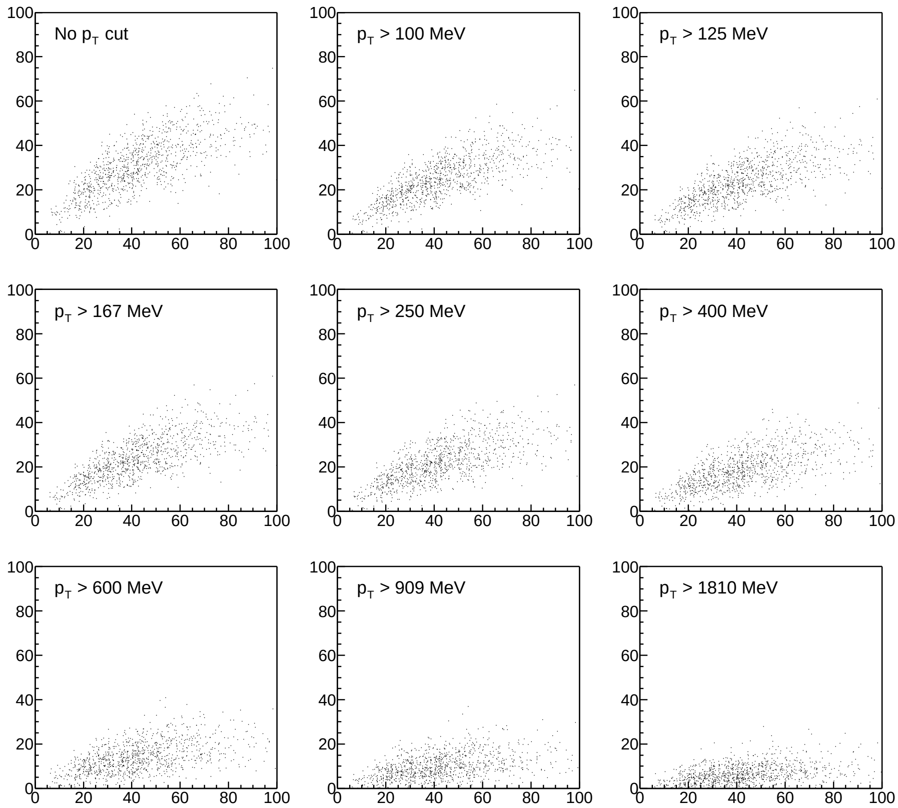

Figure 4.12: The number of segments found by the z-algorithm after applying the p_{T} cut (vertical axis) is compared to the number of L1 $r-\phi$ segments without p_{T} cut (horizontal axis). Every dot corresponds to one of 1000 AROMA Monte Carlo events.

4.5.3 Track resolution

To check the quality of the track linking step, the distance between the intersect with the z-axis and the offline reconstructed vertex is filled into a histogram for every link. The resulting shape can be described by the sum of two Gaussian distributions, one describing the combinatorial background and one the single track resolution. See figure 4.13 and table 4.3 for details. The track resolution in the AROMA Monte Carlo is $\approx 11\,\mathrm{cm}$.

4.5.4 Vertex resolution

The vertex resolution - defined as the variance σ of the distribution of the distances between the 'Top Peak' in the vertex histogram and the offline reconstructed vertex - should be better by approximately a factor $\frac{1}{\sqrt{N_{links}}}$ than the single link resolution, if the combinatorial background is effectively suppressed. Figure 4.14 suggests that this is the case for low link multiplicities. However at medium and high link multiplicities, the

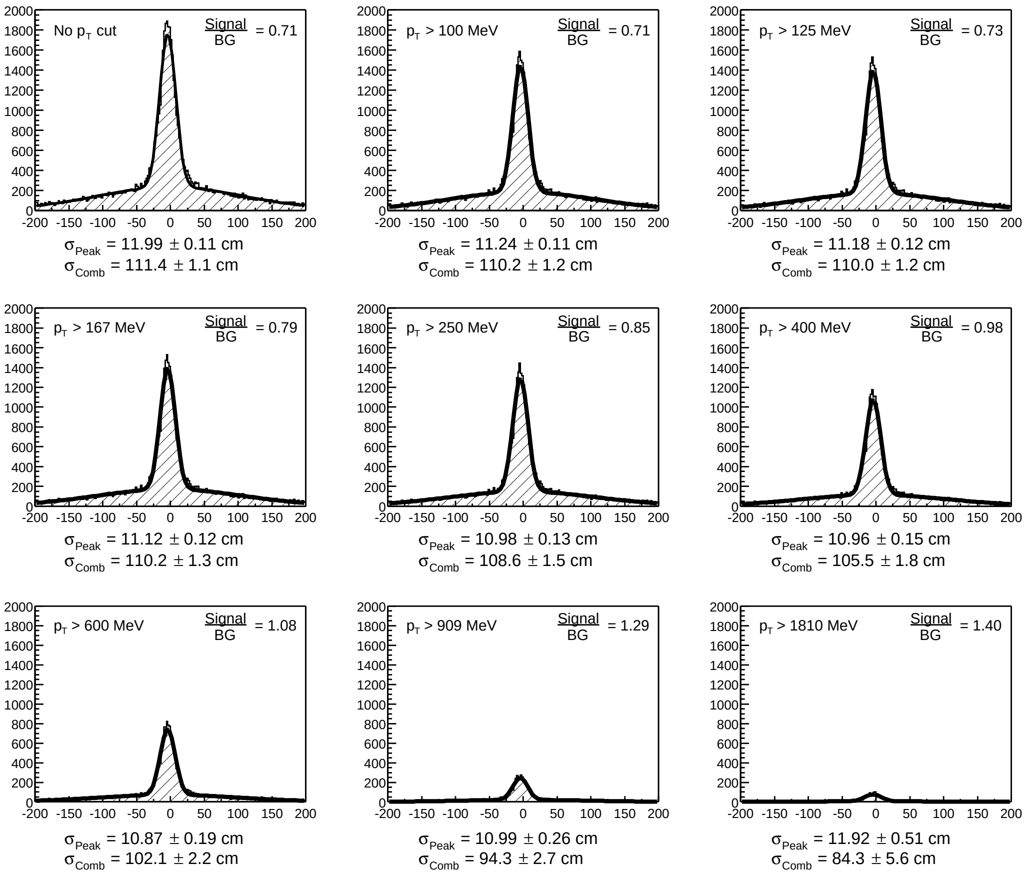

Figure 4.13: For 1000 AROMA Monte Carlo events, the distance between all link intersects and the offline reconstructed vertex is filled into a histogram; the horizontal axis represents the distance in cm, the vertical axis the number of histogram entries. The histogram is fitted with the sum of two Gaussians, one representing the combinatorial background and one the real link resolution. All possible p_{T}-cuts are applied.

resolution is limited by the finite bin size of the vertex histogram. See also table 4.3.

4.5.5 Trigger concept

The final trigger strategy should be such that the rate of ep events rejected is minimised, whilst the background rejection rate is high enough to justify using the trigger in the first place. In addition, the trigger efficiency should not decrease too much under adverse circumstances, i.e. if calibration constants are slightly wrong or parts of the CJC do not work. The background rejection power and the efficiency of the three deciding methods studied are shown in figures 4.16, 4.17 and 4.18 respectively. Except for the 'Counting Entries' method, all deciders reach efficiencies above 99%; the few permille of wrongly

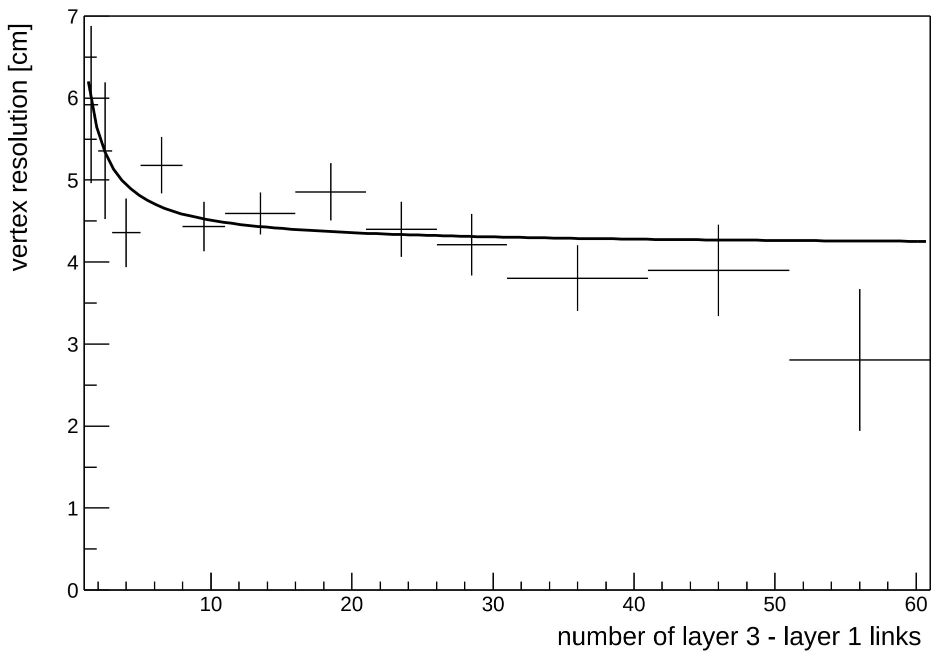

Figure 4.14: For 1000 Monte Carlo events, the average distance from the 'Top Peak' to the offline reconstructed vertex and its standard deviation are plotted dependent on the number of links between trigger layer 3 and trigger layer 1. This number is approximately proportional to the number of tracks. The line represents a fit to these points with $\sqrt{\sigma_{bin}^2 + \frac{\sigma_{track}^2}{N_{tracks}}}$, where σ_{bin} and σ_{track} are the two parameters of the fit, σ_{bin} representing the effect of the vertex histogram bin size and σ_{track} being the average resolution for single track events. The fit gives $\sigma_{bin} = 4.20 \pm 0.18\,\mathrm{cm}$ (larger than the expected $\frac{binsize}{\sqrt{12}} = 2.9\,\mathrm{cm}$) and $\sigma_{track} = 5.2 \pm 1.2\,\mathrm{cm}$ (compatible with the expected $\frac{\sigma_{link}}{\sqrt{3}} = 5.8\,\mathrm{cm}$).

rejected events are partly due to overlay (a background interaction took place in the same bunch crossing) and partly due to combinatorics conspiring to fake a vertex (usually in the forward direction). The background rejection power reaches 80% or more on the 1996 background, which was triggered by L1 triggers only. The difference between the '$\frac{3}{4}$ Peak' and the 'Top Peak' method is on the permille level. It appears that the '$\frac{3}{4}$ Peak' method is slightly more efficient for very high track multiplicity events, but it is not possible to make a definite judgement due to limited statistics.

Various discussions with H1 trigger experts [23, 24] have indicated that besides the z vertex trigger also a negative decision in the form of a veto was desired. This can be easily constructed by demanding e.g. a 'Top Peak' outside of the physics region and at least a certain number of entries in the vertex histogram (two entries should be sufficient). This veto has the same efficiency for data as the 'Top Peak' trigger; the rejection power

Sample	Single link resolution	Vertex resolution
Open charm MC	$14.83 \pm 0.13\,\mathrm{cm}$	$5.6 \pm 0.1\,\mathrm{cm}$
Neutral current	$20.17 \pm 0.18\,\mathrm{cm}$	$8.7 \pm 0.2\,\mathrm{cm}$
J/Ψ	$17.16 \pm 0.18\,\mathrm{cm}$	$7.3 \pm 0.2\,\mathrm{cm}$
b-μ	$19.58 \pm 0.19\,\mathrm{cm}$	$6.7 \pm 0.2\,\mathrm{cm}$

Table 4.3: Single link and vertex resolution for various physics cases with a p_{T} cut of 100 MeV, using the hit reconstruction algorithm.

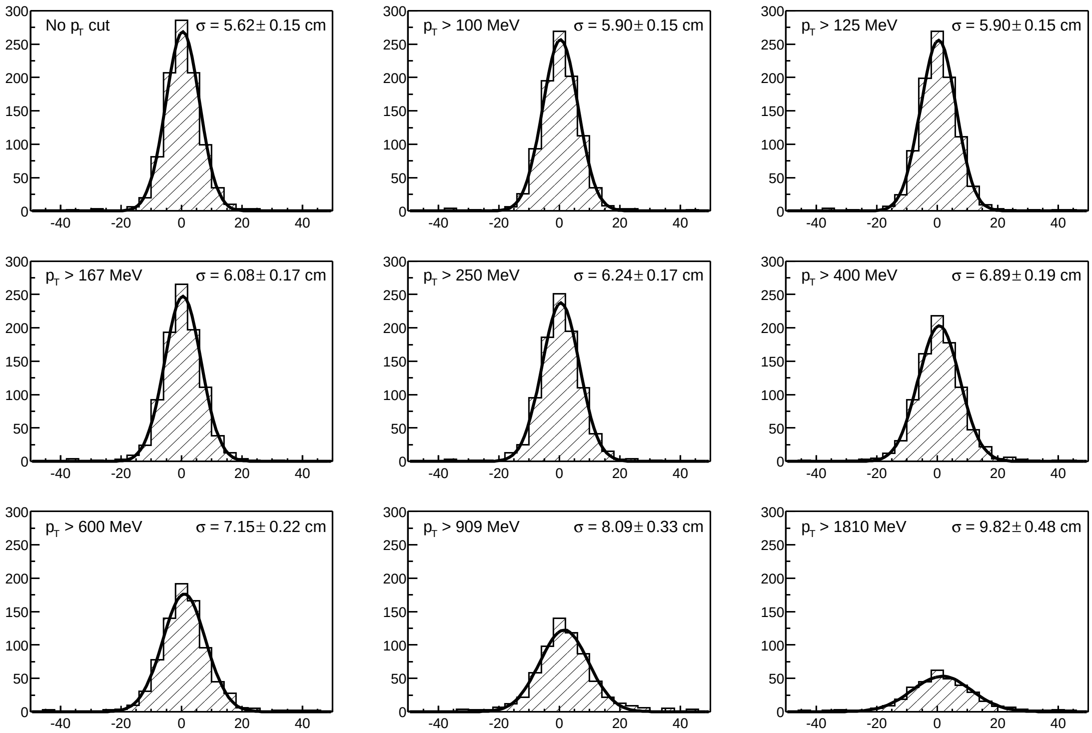

Figure 4.15: For 1000 AROMA Monte Carlo events, the distance between the 'Top Peak' position (bin with most entries in the vertex histogram) and the offline reconstructed vertex is plotted in cm. A Gaussian fit is performed to determine the resolution σ. At high p_{T}-cuts, a significant fraction of the events produces no entries in the vertex histogram.

is similar, if slightly lower as a minimum number of segments has to be present. With the 2002 data, about eighty percent of the events with an FTT t_0 and an offline reconstructed vertex outside of the physics region are rejected (figures 4.19, 4.20). For positron and proton only runs, the rejection power is decidedly higher but becomes comparable if only events with tracks are studied (figure 4.21).

As the decider algorithms (except the 'Counting Entries' method) have a very similar

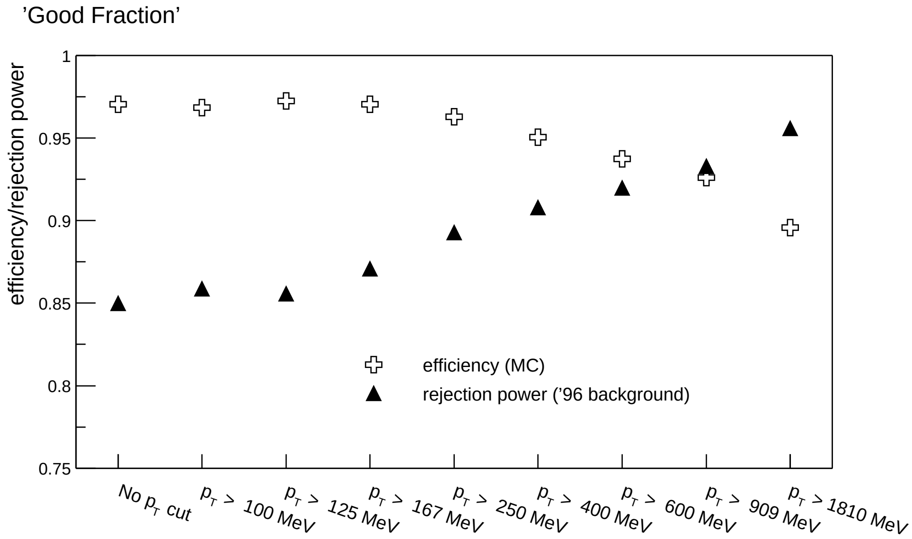

Figure 4.16: For 1000 events each of AROMA MC and 1996 background, the efficiency and background rejection power of the 'Good Fraction' method are determined dependent on the p_{T} cut.

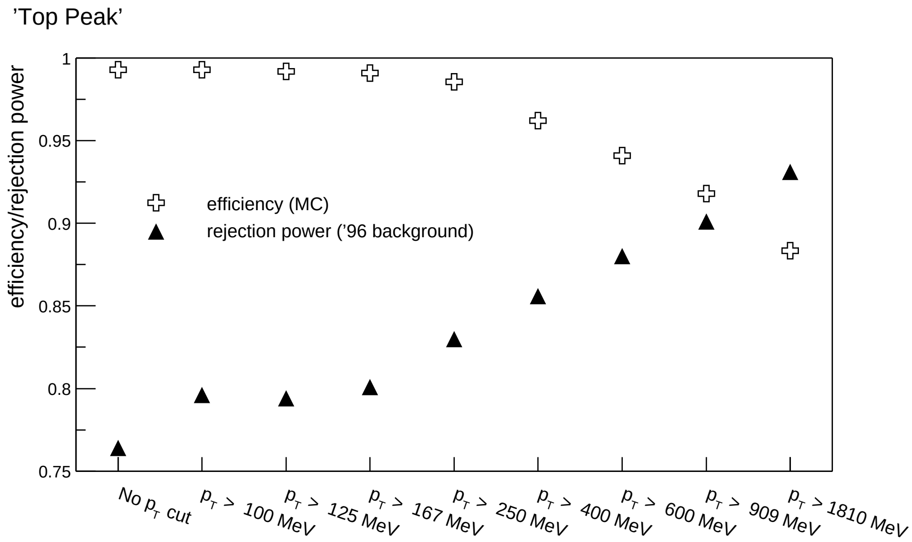

Figure 4.17: For 1000 events each of AROMA MC and 1996 background, the efficiency and background rejection power of the 'Top Peak' method are determined dependent on the p_{T} cut.

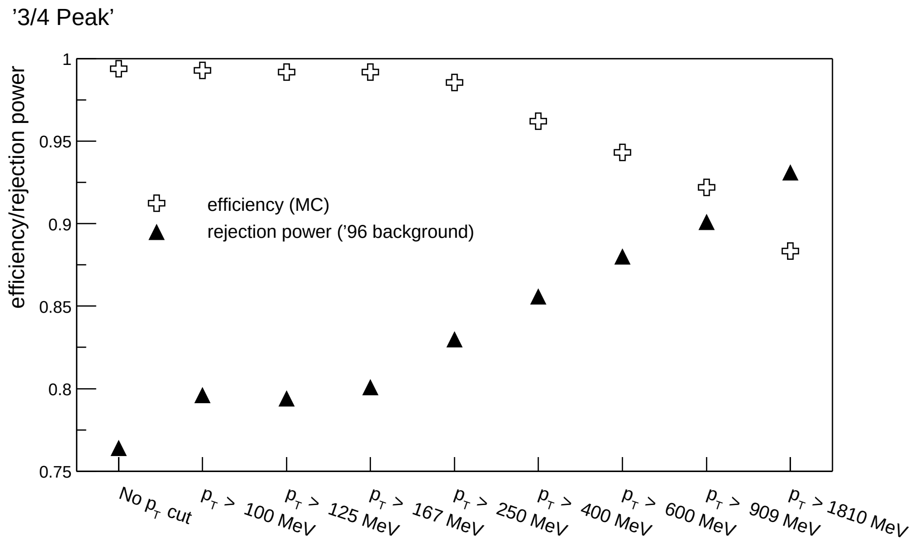

Figure 4.18: For 1000 events each of AROMA MC and 1996 background, the efficiency and background rejection power of the '$\frac{3}{4}$-Peak' method are determined dependent on the p_{T} cut.

performance, it is difficult to give a final recommendation on which one to use; the 'Top Peak' method is slightly simpler than the '$\frac{3}{4}$ Peak' one, the latter has on the other hand proven to be more stable when the whole simulation was run inadvertedly with a set of completely wrong calibration constants. The algorithm is also quite robust if even large parts of the CJC are out of order (figure 4.22). If bad running conditions demand a higher background rejection power, it appears advisable to tighten the physics region instead of the p_{T} cut, as this won't introduce a bias against specific event topologies (low p_{T}, low track multiplicity) but rather decrease the efficiency across the whole spectrum of physics cases (figures 4.23, 4.24). Part of these decisions can be delegated to the central trigger, as up to eight trigger elements with different acceptance regions can be sent, however the p_{T} cut has to be fixed, as it is performed early in the algorithm and there is no possibility to transmit p_{T} information to the decider card.

4.5.6 The 'Segment slope' algorithm

As figure 4.25 shows, background events contain on average a lot more segments in the backward part of the CJC that are tilted away from the interaction region than signal events do. For the forward part of the CJC one would expect the same, but as high track multiplicity events with a vertex in the far forward region are extremely rare, they are difficult to study and there is no urgent need to veto them. As the trigger decision has of course to be taken on an event by event basis, the cut has to be laid such that no

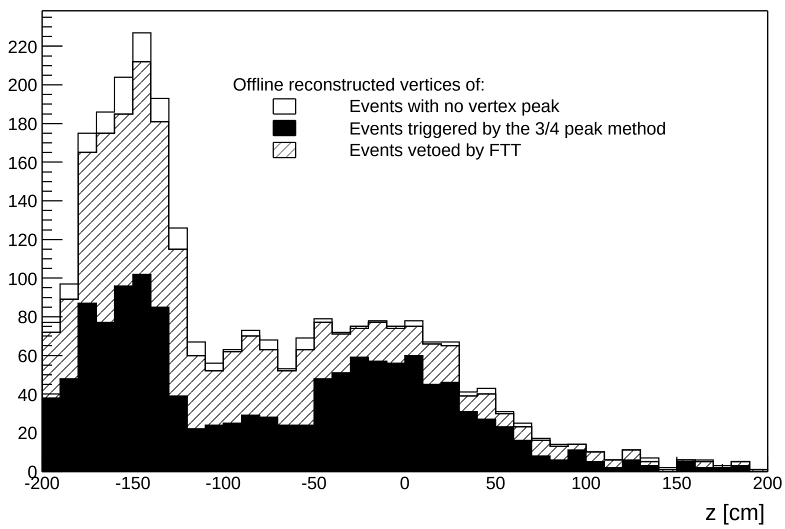

Figure 4.19: For 4700 events from the first day of 2002 luminosity operation, the offline reconstructed vertices of those events which contain tracks, of FTT z-vertex simulation triggered ($\frac{3}{4}$-peak method) and vetoed events are plotted on top. More than 2000 events do not appear in the plot, as they contain only synchrotron radiation hits and no tracks. Note that the collimators at -150 cm and -80 cm are visible whereas a peak from ep events in the nominal interaction region is not. The triggered events outside of the signal region as well as the vetoed events within that region are mainly due to overlays (more than one vertex per event) and pileup (tracks from more than on bunch crossing).

or only extremely few signal events are lost. This in turn leads to the fact that (when defining a veto region as shown in figure 4.25) only about 5% of the background events can be rejected. The veto power is consequently very limited and so the segment slope information would only be useful for triggering in conjunction with additional indicators. A use for the FTT L1 z-vertex trigger is not easily possible anyway, as there is no free transmission capacity in the L1 merger chain.

4.6 Summary

The presented z-vertex trigger algorithm provides a relatively straightforward and very robust tool for rejecting a large variety of background whilst keeping a high efficiency for all kinds of physics events. The 'segment slope' algorithm on the other hand is of no use as a level 1 trigger but helped to understand the segment finding step and shows that there is still some unused information hidden in the signals used for the FTT.

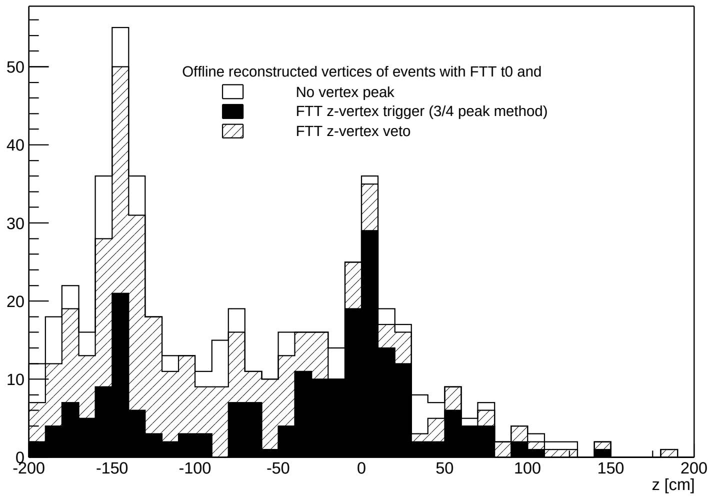

Figure 4.20: For 4700 events from the first day of 2002 luminosity operation the offline reconstructed vertices of all 518 events with a simulated FTT t_0 are shown. The events with a simulated z-vertex trigger ($\frac{3}{4}$-peak method) and veto respectively are shown on top. Note that the FTT t_0 enhances the peak at $z = 0\,\mathrm{cm}$ which was not easily visible in figure 4.19.

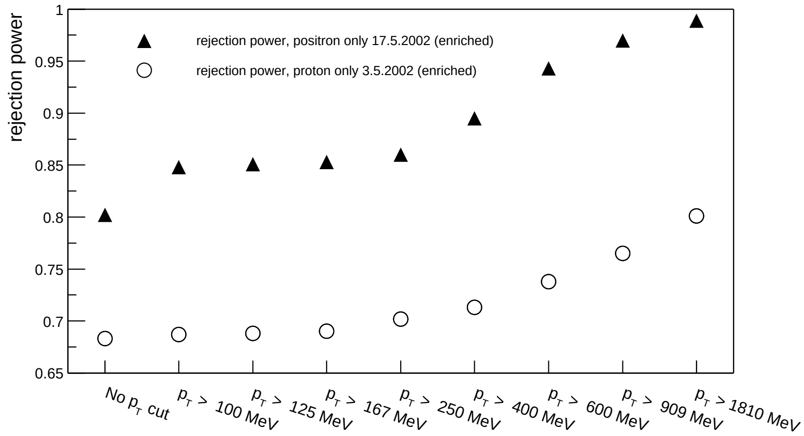

Figure 4.21: For 1000 events with tracks of a proton only and a positron only file the rejection efficiency is determined for various p_{T} cuts using the '$\frac{3}{4}$-Peak' method. For the protons, no offline reconstructed vertices were available, so also events with vertices in the interaction region enter into the rejection power.

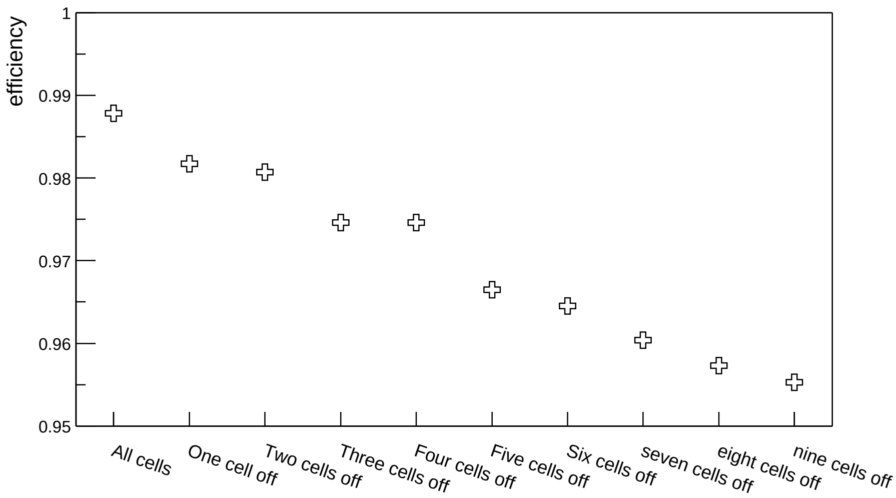

Figure 4.22: For 1000 AROMA Monte Carlo events, the decrease in trigger efficiency of the '$\frac{3}{4}$-Peak' method is plotted if adjacent cells of the CJC are switched off one after the other. Note that even with 'all cells' the CJC is not at its maximum efficiency, as the Monte Carlo was generated using a table of defect wires for a specific running period.

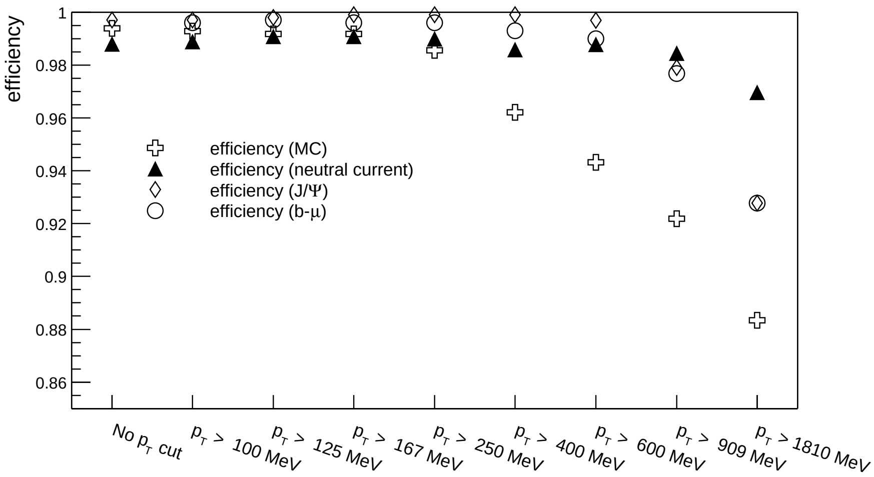

Figure 4.23: For 1000 events from several physics samples, the efficiency of the '$\frac{3}{4}$-Peak' method is determined dependent on the p_{T} cut. See table 4.2 for details on the samples.

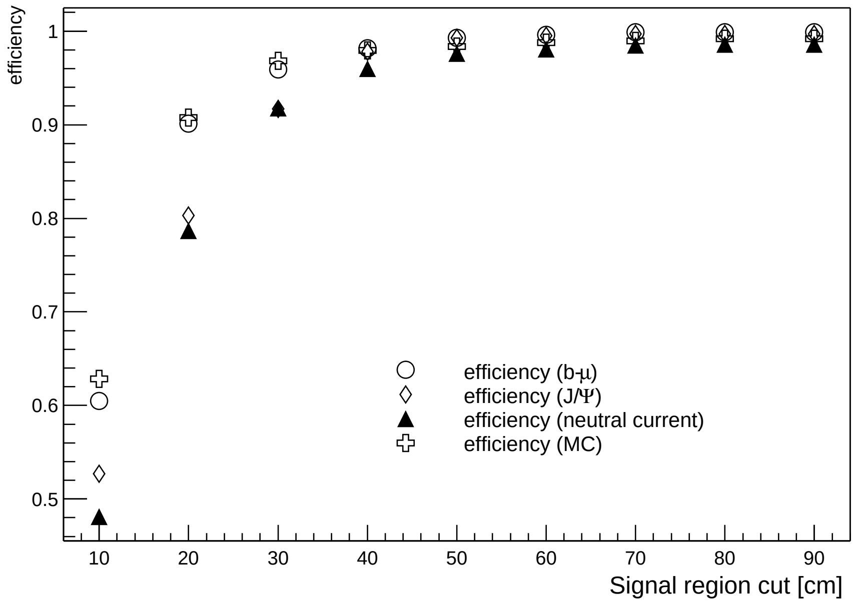

Figure 4.24: For 1000 events from several physics samples, the efficiency of the '$\frac{3}{4}$-Peak' method is determined dependent on the signal region cut. See table 4.2 for details on the samples.

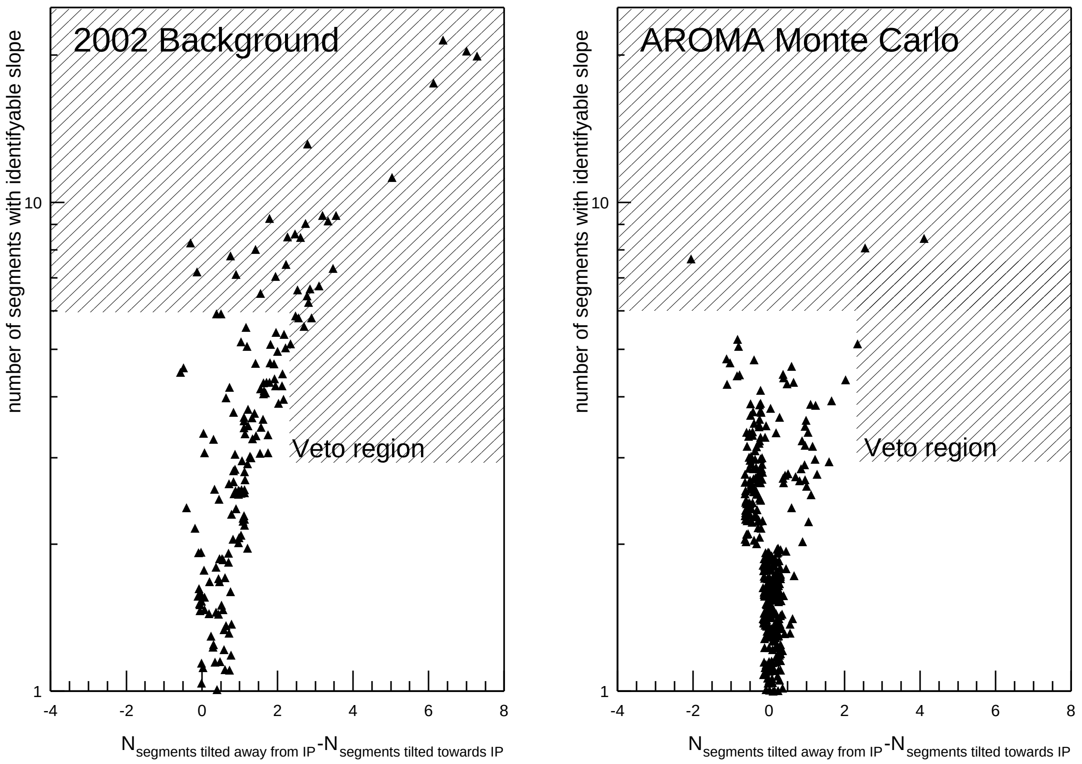

Figure 4.25: For 1000 AROMA Monte Carlo events and 5000 2002 background events, the number of segments in the backward part of the CJC with an identifiable slope is counted. This number is plotted versus the number of segments tilted away from the nominal interaction point minus the number of segments that are tilted towards this point. Every triangle corresponds to one event. A possible veto region is indicated with the shaded area.

Chapter 5

A fast and accurate z-vertex determination for the level 2 FTT

5.1 Motivation

The precise pseudo 3D ($r-\phi$ and $r-z$) track fit performed by the DSPs of the level 2 Fast Track Trigger uses a vertex constraint, i.e. assumes a common origin of the tracks. The x and y positions lie within the very small ($\lesssim 100\,\mu$m) beamspot, whose position is accurately known. The z position of the vertex however varies from event to event, as the proton bunches have a length of $\approx 30\,$cm. Some additional input to the fitter is therefore required.

In the original FTT proposal, the peak position in the histogram of the 'old' (pre CIP2000) z-vertex trigger with signals from the new CIP was foreseen as input. With a bin size of $\approx 5\,$cm it has a considerably higher resolution than the FTT L1 z-vertex histogram as proposed in this thesis. As the CIP2000 and the corresponding trigger (histogram bin size: $16-20\,$cm) was still in the commissioning phase at the time of writing, there was as yet no experience concerning data quality or average uptime of that system available and it was also not clear whether the new chamber would work with the old trigger hardware.

As $r-z$ information is available to the FTT, it is desirable to perform an additional precise z-vertex determination, either to resolve ambiguities and to increase accuracy if there is input from the CIP or to provide some redundancy if the CIP is not operational.

5.2 Algorithm

5.2.1 Overview

On each of the six L2 fitter cards there are 4 DSPs which perform the track fits. The first 24 (or less, in case of low track multiplicity) tracks found by the L2 linker are distributed amongst the DSPs which perform first the $r-\phi$ and then the $r-z$ fit for one track each. In a second round, the same is repeated with the remaining tracks (again up to 24). During the first $r-\phi$ fit, there is enough time to determine a z vertex position which can then be used for the $r-z$ fits.

The segments belonging to the first 24 linked tracks are consequently available as an input to the algorithm described below. As the z measurement by charge division is not as accurate as the rest of the Qt algorithm and may be disturbed in the case of multiple hits on the same wire, an outlier rejection ensures that the z values used in a single track fit are consistent. For every track a simple pseudo-fit is performed, approximating the method of least squares, but without iterations or complicated and time consuming higher mathematical functions. The simple algorithm allows a fast implementation in an FPGA, thus ensuring that the result is available in time for the $r-z$ fit and making optimal use of the free resources on the fitter cards. The intersects of the tracks with the z axis are then calculated and a peak finder is used to identify tracks not originating from the primary vertex. Finally, the vertex position is determined as an average of the intersects of the 'good' tracks.

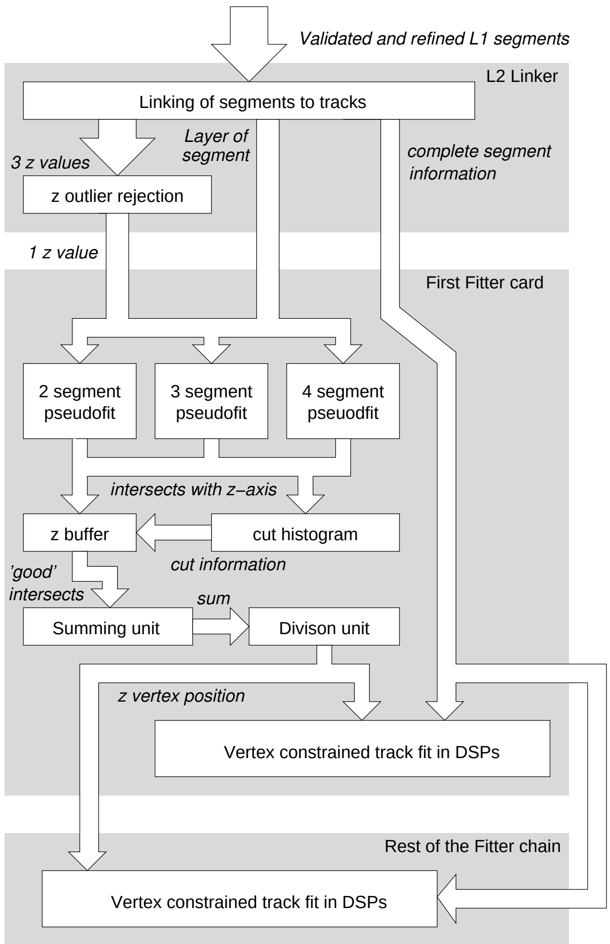

Figure 5.1: Flow diagram of the L2 z vertex finder algorithm.

5.2.2 z-outlier rejection

For every $r-\phi$ track segment, three hits are required, and therefore three z values should be available. As the charge division technique used to measure the z coordinate of a hit is more easily affected by for example ADC overflows caused by multiple hits on one wire than the $r-\phi$ Qt analysis, quite a few z measurements are inaccurate or even wrong. To deal with these, a check is performed whether the three values are consistent, and if not, outliers are rejected. This is done using the ingeniously simple and fast *First Look* technique due to J. Samson [25]: first middle one of the three z values is identified, second the distance of the other two hits to the central one is compared with a predefined cut, if above it, the respective z value is rejected. If all three hits are inconsistent, the whole segment is rejected. It is still open, whether the z outlier rejection will be performed on the FEM or on the L2 Linker. After the outlier rejection the average of the valid z positions is calculated. As the z values are represented by 6 bit (62 valid values, 3.55 cm bin size) it appears appropriate to store the average position with 7 bit accuracy (126 valid values, 1.75 cm bin size).

5.2.3 Track fit

In the magnetic field of the H1 detector, charged particles follow a helix trajectory. The projection of the helix onto the $r-z$ plane is a sine. In principle, the track fit should therefore be performed in the $s-z$ plane (s is the arclength along the sine) where the tracks are straight lines. The transformation from r to s is described by

$$s = 2 \cdot \frac{\arcsin\left(\frac{\kappa \cdot r}{2}\right)}{\kappa}. \tag{5.1}$$

It is difficult and needs a lot of resources to perform this calculation in full in an FPGA. It could quite easily be done using a lookup table of pre-calculated values. But even this is not necessary: More than half of the segments have an r to s difference of less than 1 mm and for over 95% of the segments, the correction is smaller than 2 cm. This is comparable or smaller than the smearing that is introduced by the binning of the digitisation. The effect on the vertex resolution of omitting the r to s transformation is of the size of a few tenths of a mm, and therefore utterly negligible.

A linked track can consist of two, three or four segments and depending on the segment number, the pseudo-fit takes a different form.

Two segments

For two segments, the 'track fit' is straightforward: In the $r-z$ plane, the positions of the two segments are extrapolated to the z-axis:

$$z(r=0) = z_2 + r_2 \cdot \frac{z_1 - z_2}{r_1 - r_2} \tag{5.2}$$

where the indices denote the inner and outer segment respectively.

Three segments

With three segments, an easy method coming very close to a fit with the method of least squares is chosen (in fact it is even identical to a fit to equidistant points with equal errors): the outer two segments define the slope of the track which is then shifted so that it passes through the centre of gravity of all three segments:

$$z(r=0) = \frac{z_1 + z_2 + z_3}{3} + \frac{r_1 + r_2 + r_3}{3} \cdot \frac{z_1 - z_3}{r_1 - r_3} \tag{5.3}$$

where the indices denote the inner, middle and outer segment respectively.

Four segments

For the case with four segments, it seems natural to calculate two slopes, form a mean and lay a track with the mean slope through the centre of gravity of all four segments. There are essentially three possibilities (figure 5.2): combining the inner and outer pair of segments (equation 5.4), combining 1 and 3 and 2 and 4 respectively (equation 5.5) and finally forming a weighted mean of the slope obtained from the innermost and outermost and the middle segment (equation 5.6):

$$z(r=0) = \frac{z_1 + z_2 + z_3 + z_4}{4} + \frac{r_1 + r_2 + r_3 + r_4}{4} \cdot \frac{\frac{z_1 - z_2}{r_1 - r_2} + \frac{z_3 - z_4}{r_3 - r_4}}{2} \tag{5.4}$$

$$z(r=0) = \frac{z_1 + z_2 + z_3 + z_4}{4} + \frac{r_1 + r_2 + r_3 + r_4}{4} \cdot \frac{\frac{z_1 - z_3}{r_1 - r_3} + \frac{z_2 - z_4}{r_2 - r_4}}{2} \tag{5.5}$$

$$z(r=0) = \frac{z_1 + z_2 + z_3 + z_4}{4} + \frac{r_1 + r_2 + r_3 + r_4}{4} \cdot \frac{3 \cdot \frac{z_1 - z_4}{r_1 - r_4} + \frac{z_2 - z_3}{r_2 - r_3}}{4} \tag{5.6}$$

where the indices denote the four segments inward out. Not surprisingly, the second and third method are more accurate than the first; one of them has to be chosen for the actual implementation - the second method has the advantage, that the additional multiplication with three is not needed and was therefore selected (see table 5.1). As the four radii

Pseudo-fit	RMS [cm]	σ [cm]
1-2 and 3-4	5.41	4.74 ± 0.17
1-3 and 2-4	3.67	2.46 ± 0.09
3×1-4 and 3-4	3.70	2.43 ± 0.08

Table 5.1: Single track resolution RMS and σ for three different four segment pseudo-fits.

are constant, all the 'divisions' in the above equations are in fact multiplications with a constant, which the FPGAs used for the FTT can perform within a single processing cycle. All in all, there are eleven such multiplications possible, one for the four segment, four for the three segment and six for the two segment case.

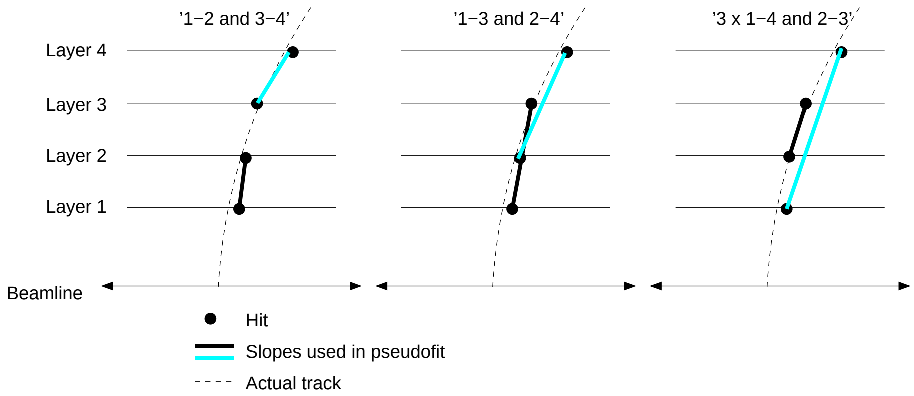

Figure 5.2: The three possible slope combinations for the four segment pseudo-fit.

5.2.4 Excluding tracks not originating from the primary vertex

All the $z(r = 0)$ values obtained in the pseudo fits are buffered and at the same time entered into a 32 bin *cut histogram*, covering a region from $z = -60$ cm to $z = +60$ cm. A peak is searched for and all the z values not lying in the peak bin or its neighbours (a total of 11.25 cm) are ignored.

5.2.5 Calculating an accurate vertex position

The remaining z values are used to form a weighted sum, the weights being determined by the number of segments entering at a z position[1]. This sum is then divided by the sum of the weights and the resulting z position is used for the fit. As the single track resolution is a few cm, for high multiplicity events the vertex resolution can at maximum be a factor of $\frac{1}{\sqrt{24}}$ better,[2] motivating a 7 or even 8 bit output (0.94 cm and 0.47 cm bin size in the $z = -60$ cm to $z = +60$ cm signal region).

5.3 Hardware implementation

The L2 algorithm would be implemented on the 'data controller' FPGA of the first L2 fitter card. Except for the final division (which also takes not more than three or four processing cycles), only fast linear operations are used. The result should therefore be available in time for the $r-z$ fit even in cases where the linking takes longer than average.

[1]A possible enhancement of the algorithm would be the introduction of weights that depend also on the lever arm.
[2]The L2 linker links at most 24 tracks in the first round.

5.4 Simulation

The simulation was performed within the same framework that was also used for testing the L1 algorithm. Refer to section 4.4 for details.

5.5 Performance

In the following sections it will be shown, that with a careful optimisation of the algorithm, a vertex resolution of the order of 2 cm is obtainable (see figure 5.3).

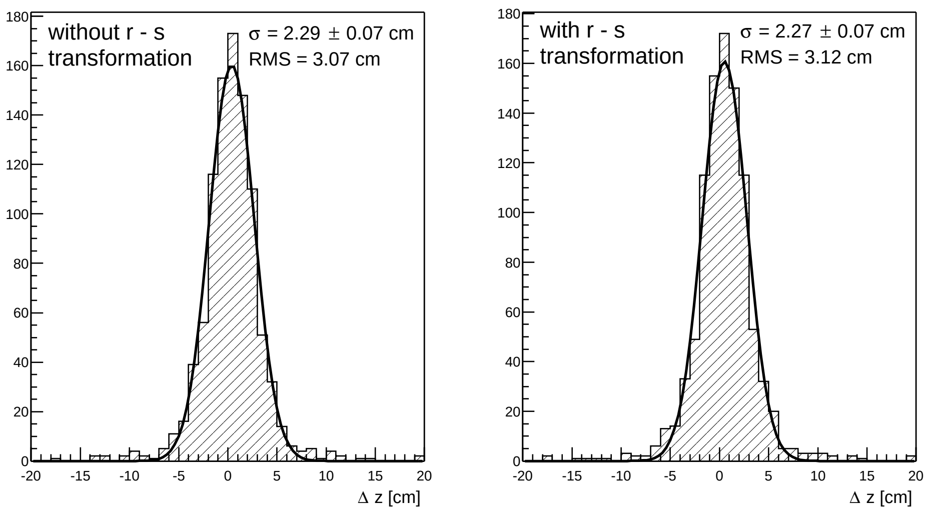

Figure 5.3: For 1000 AROMA Monte Carlo events, the distance between the FTT vertex and the offline reconstructed vertex is calculated, on the left without and on the right with the r-s transformation. The resulting histograms are fitted with a Gaussian. The difference between both methods is smaller than the error of the fit.

5.5.1 Outlier rejection

The *First Look* outlier rejection method was found to give the best fit results (for the track angle θ) with a cut of about 15 cm [25]. For vertex finding, a tighter cut might be desirable (see figure 5.4), but as the effects of the cut size are rather small, it appears appropriate to optimise the cut for the fit rather than for the vertex determination. The effect of the cut as such, on the other hand, is significant, as badly measured or wrongly linked hits are prevented from givinging tails in the z resolution function.

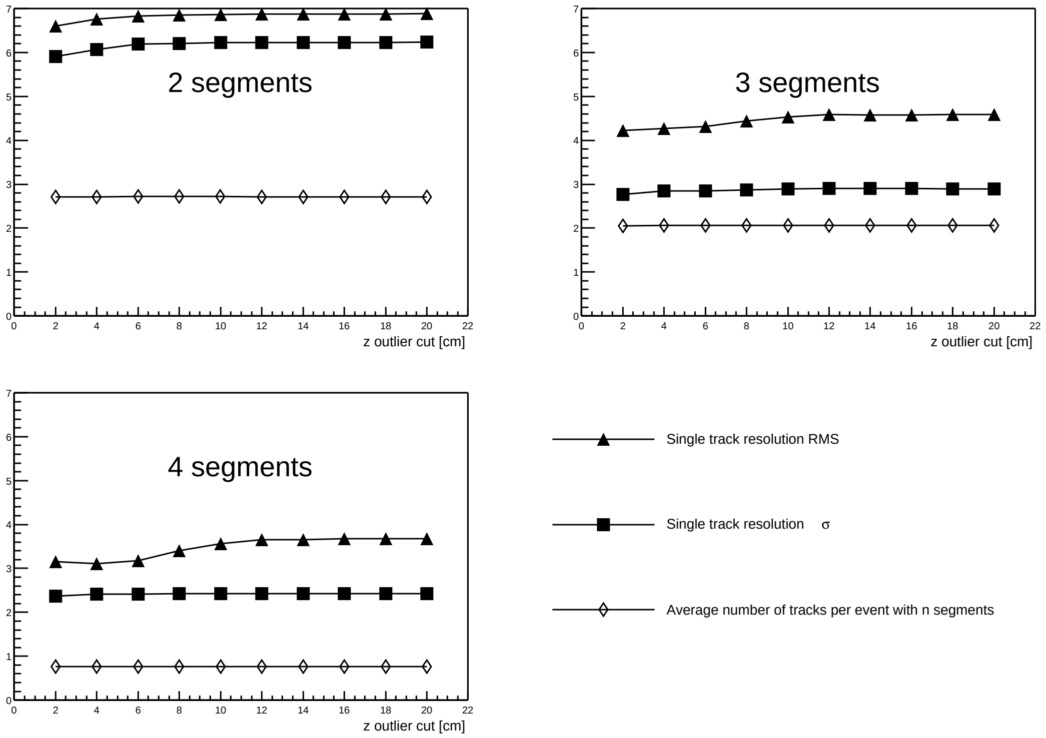

Figure 5.4: For 1000 AROMA Monte Carlo events, the distance between the intersect of the tracks with the z axis and the offline recalculated vertex is determined. RMS and σ of this distribution are calculated and entered into the graph together with the average number of tracks per event with a given number of segments. It can be seen that the resolution is only weakly dependent on the cut and that even with very tight cuts, almost no tracks get lost.

5.5.2 Track fit

As can be seen from figure 5.3, the r-s transformation does not significantly increase the vertex resolution and is therefore omitted[3].

The track pseudo-fit accuracy improves dramatically with the number of segments, as can be seen in figures 5.4 and 5.5. It is therefore advisable to use large weights for tracks with more segments in the final sum. As there is a considerable amount of events containing only two segment tracks and as they are most frequent, they cannot be excluded from the sum despite of their relative inaccuracy.

[3]This could be problematic for event topologies with only low momentum tracks (e.g. a ϕ meson decaying to two slow Kaons).

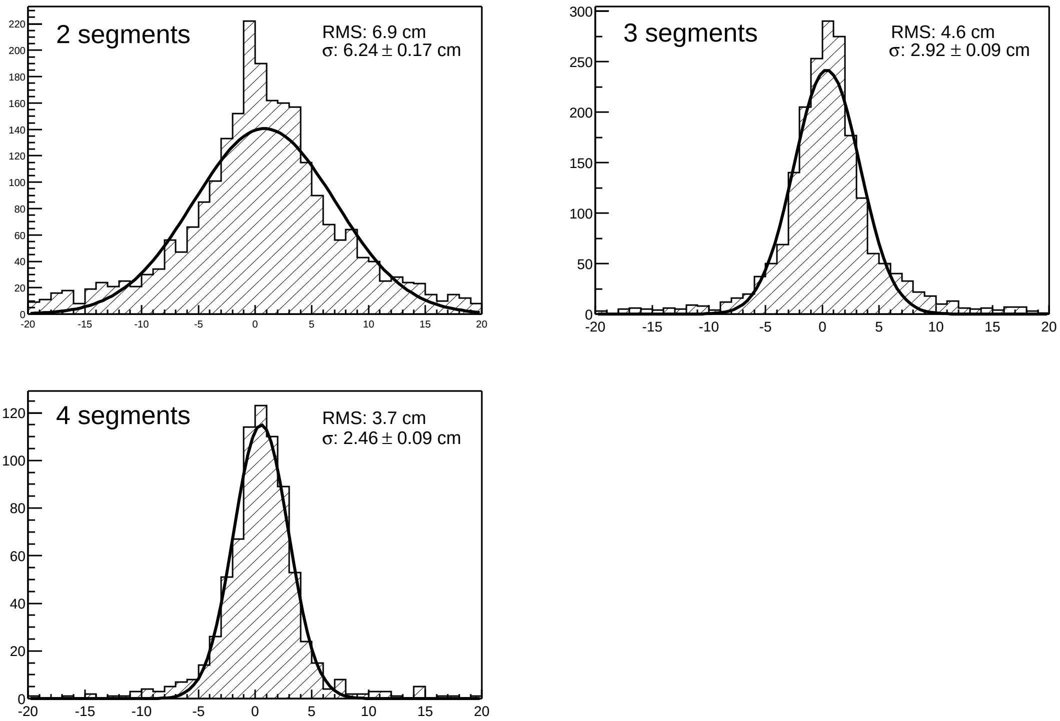

Figure 5.5: For 1000 Monte Carlo events, the distance between the intersect of the track with the z axis and the offline recalculated vertex is entered into a histogram. The histograms are fitted with a Gaussian. In the case of the two segment tracks, the shape is a superposition of several Gaussians due to the different lever arms between segments at different radii.

5.5.3 Excluding tracks not originating from the primary vertex

All tracks with an intersect outside the signal region of $\pm 60\,\mathrm{cm}$ are not considered in the vertex position calculation. An additional cut is performed with the cut histogram, whose bin size can be adjusted to give an optimal resolution (tracks not originating from the primary vertex should be rejected, but the cut should accommodate as much 'good' tracks as possible to increase the accuracy of the mean). Figure 5.6 shows that a the optimum is somewhere between 20 and 40 bins. For the implementation in an FPGA a 32 bin histogram is probably the optimum, as it uses the available resources efficiently and allows a 1:4 or 1:8 correspondence between the cut histogram bins and the final 7 or 8 bit output.

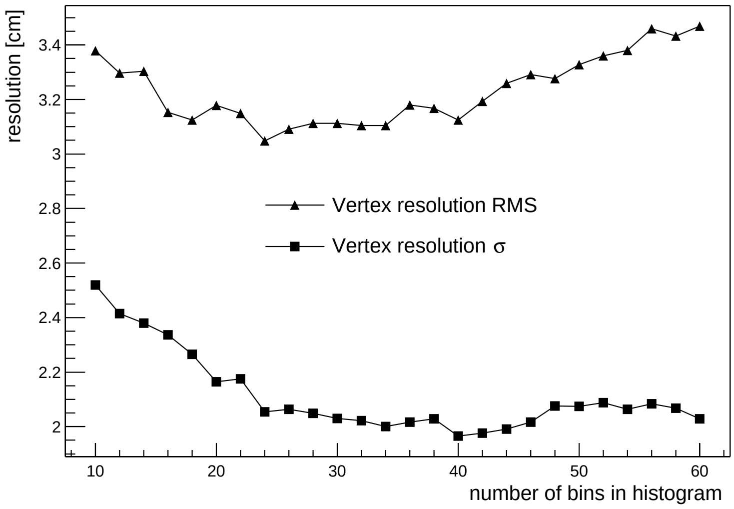

Figure 5.6: For 1000 AROMA Monte Carlo events, the vertex resolution RMS and σ are plotted for various bin numbers in the cut histogram.

5.5.4 Calculating an accurate vertex position

For the final sum and division it is important to find sensible factors to weight tracks with, according to their respective accuracy. In the framework presented here, it was found that weighting 2, 3 and 4 segment tracks with factors of 1, 2 and 6 respectively gives a more accurate vertex position than any other combination of three weights all smaller 10.

The vertex resolution as a function of the number of tracks is shown in figure 5.7. It follows very neatly the expected $\frac{a}{\sqrt{N_{Tracks}}}$ curve. The fact that timing constraints allow only 24 tracks to be used for the z vertex determination does not significantly deteriorate the resolution, as on one hand the number of very high track multiplicity events is small and on the other hand the expected improvement when going from 24 to 48 tracks is merely a factor of $\frac{1}{\sqrt{2}}$ and so the theoretically obtainable resolution in a 48 track event is about 1.4 cm as opposed to 2 cm.

5.6 Summary

To conclude, it is possible to identify the interaction vertex with FTT data alone to an accuracy of about 2 cm, thus either replacing the need for CIP input or increasing the accuracy by a significant factor, if using a combination of CIP input and FTT z-vertex determination. For quasi elastic events with just two tracks, the vertex resolution can be as bad as 6 cm, so a combination with the CIP is desirable.

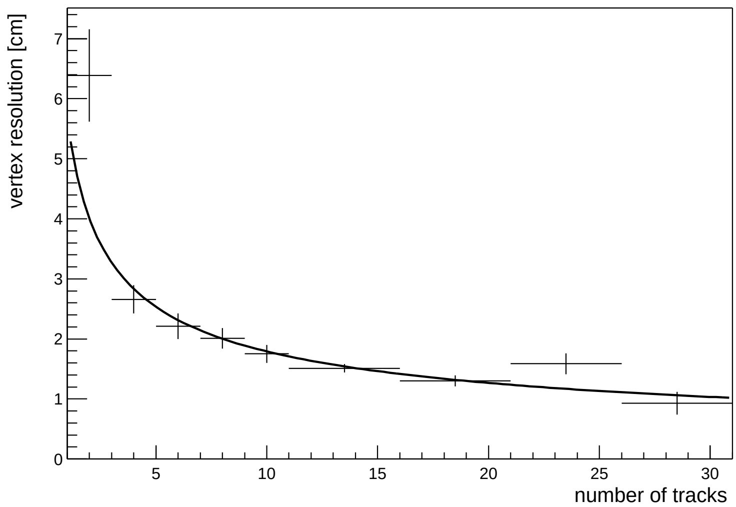

Figure 5.7: For 1000 AROMA Monte Carlo events, the average distance between the offline reconstructed vertex and the FTT vertex and its standard deviation is plotted against the number of tracks used for the vertex determination. The fit is a $\frac{a}{\sqrt{N_{Tracks}}}$ curve, where a is the single track resolution and comes out of the fit as $5.67 \pm 0.16\,\mathrm{cm}$.

Chapter 6

Conclusions

The FTT hardware with its modular design and high flexibility - mainly due to the usage of fast programmable logic - is a formidable device for pattern recognition. Not only in the $r-\phi$ plane, where hits are confined to a few hundred μm around the track, but also in the $r-z$ plane, where hits are smeared over centimetres and tracks often overlap, the FTT can identify track segments and tracks at the very high speeds needed to form trigger decisions. The L1 z vertex trigger alone is able to process and compress an input of up to 16 Gigabyte of information per second[1] down to the 10 Megabyte of trigger information sent to the central trigger logic in the form of eight trigger elements per bunch crossing.

6.1 The L1 FTT z-vertex trigger

This diploma thesis shows that it is possible to identify tracks in the $r-z$ plane of the central jet chamber by the following steps: Track segments are identified using information from the Qt algorithm. A p_{T} cut with the help of the FTT $r-\phi$ algorithm significantly increases the quality of the $r-z$ segments. These segments can be linked pairwise to tracks without the combinatorial background getting out of control. The resulting z-vertex histogram contains enough information to obtain a vertex resolution of $\approx 6\,\mathrm{cm}$ on ep events. This is sufficient to reach trigger efficiencies of 99% and more. It is also possible to reject about 80% of the background events with tracks and a vertex outside of the signal region. The algorithm is simple and very robust against CJC inefficiencies and wrong calibration. Although not explicitly tested, the algorithm is designed such that it should fulfil the tight timing restriction of the L1 trigger latency, as there are no more time consuming operations than in the $r-\phi$ part of the algorithm.

The effort for building this trigger is limited to installing one additional FTT multi purpose board and programming its FPGAs as well as extending the code in the front end module FPGAs. It is therefore a cheap and elegant addition to the CIP2000 z-vertex trigger, for which it can serve as a fallback, cross check or enhancement.

[1] 3 layers a 30 cells a 3 wires with 46 bit information each, plus 90 bit p_{T} cut information, all at the HERA frequency.

6.2 A refined z-vertex position for the L2 FTT

On the second trigger level, it is possible to determine the z-vertex position with a resolution of $\approx 2\,\mathrm{cm}$, thus potentially increasing the accuracy of the track fit and at the same time reducing the dependence on other components such as CIP and COP. Timing is less an issue than on level 1 and so more complex calculations can be performed in the FPGAs.

The implementation requires no new hardware, only FPGA programming and is planned to be part of the L2 FTT system right from the beginning of its operation.

Chapter 7

Acknowlegdments

I would like to express my gratitude to all the people who have made this thesis possible and my time at DESY both an enlightening and enjoyable experience. My thanks go to Professor Ralph Eichler for giving me the opportunity to work on the fascinating topic of the Fast Track Trigger and to Christoph Grab for his suggestion of doing a particle physics diploma.

Only the efforts of hundreds of physicists and technicians working with the H1 collaboration produced the framework I had the pleasure of working with and the various data my algorithm and I had to deal with. I would like to mention especially Daniel Pitzl, Claus Kleinwort and Carsten Niebuhr who illuminated my way through the 2002 data with many explanations and hints.

A lot of insights but also a great many enjoyable moments I owe to the Dortmund FTT group; Hans-Christian Schultz-Coulon, Christoph Wissing, Ricardo Lopez, Juergen Naumann, Olaf Behrendt, Marc-Oliver Boehnig, Martin Windisch and Andrea Vargas. A very special 'thank you' goes to Yves Fleming, who both joined me in the crusade to squash bugs in the `fttemu` code and introduced me to the gastronomical highlights of Ottensen. I also have very fond memories of Nicole Werner, Juergen Kroseberg, Benno List and Simon Baumgartner who suffered me and my *Fanta*-bottles in our office for four months and supplied me with index files, decisive lines of code and all those little hints that helped me to get my work done but also contributed to my enjoyment of Hamburg. I would also like to mention Rahel, who never gave up on her quest of finding out what exactly and - probably even more important - why I did what I have done.

Most importantly, I would like to thank André Schöning for his excellent tutorship; he has mastered to find a perfect equilibrium between showing me the way when I was in danger of getting lost and letting me search alone in the dark, when he suspected something precious hidden there. All the people mentioned, but in particular André and Benno, through displaying their great joy in physics, have contributed to my decision of dedicating also the next few years of my life to particle physics.

List of Figures

1.1 A physics and a background event 7

2.1 HERA 10
2.2 Side view of H1 12

3.1 Overview of FTT components 16
3.2 Location of trigger layers in the CJC 17
3.3 Functional layout of the Front End Module 18
3.4 A shift register 19
3.5 The Shift Register concept 19

4.1 The L1 z-vertex system 27
4.2 Geometry of trigger wires in CJC1 28
4.3 The pipelines used to account for drift times. 29
4.4 The z finder sliding window 29
4.5 Reconstruction of track curvature 30
4.6 A sector in ϕ 31
4.7 The $r-z$ linking algorithm 32
4.8 Geometrical acceptance of the FTT z-vertex trigger and the CIP2000 33
4.9 The segment slope classification 34
4.10 The merger chain 35
4.11 Bin size dependence of the segment finding 37
4.12 z segment finding efficiency vs. $r-\phi$ segment finding efficiency 38
4.13 Single link resolution as a function of the p_{T} cut 39
4.14 Vertex resolution versus number of tracks 40
4.15 Vertex resolution as a function of the p_{T} cut 41
4.16 Efficiency and rejection power as a function of the p_{T} cut for the good fraction method 42
4.17 Efficiency and rejection power as a function of the p_{T} cut for the top peak method 42
4.18 Efficiency and rejection power as a function of the p_{T} cut for the $\frac{3}{4}$-peak method 43
4.19 Vertex distribution of triggered and vetoed events in 2002 data 44
4.20 Vertex distribution of triggered and vetoed events in 2002 data with FTT t_0 45

4.21 Rejection power for positrons and protons alone 45
4.22 Efficiency with reduced CJC capabilities 46
4.23 Efficiency as a function of the p_T cut for various physics samples 46
4.24 Efficiency as a function of the signal region cut for various physics samples 47
4.25 Distribution of segment slopes 48

5.1 Overview of the L2 algorithm 50
5.2 The three possible slope combinations for the four segment pseudo-fit . . . 53
5.3 Vertex resolution with and without r-s transformation 54
5.4 Single Track resolution versus z outlier cut 55
5.5 Single Track resolution of tracks with 2, 3 and 4 segments 56
5.6 Vertex resolution versus cut histogram bin size 57
5.7 Vertex resolution versus number of tracks 58

List of Tables

2.1 Design parameters of HERA II 10
2.2 H1 detector components 13

3.1 L1 trigger elements 20
3.2 L2 trigger elements 23

4.1 A possible set of L1 z-vertex trigger elements. 33
4.2 Datasets used for performance tests and tuning 36
4.3 Link and vertex resolution for different physics cases 41

5.1 Resolution of three different four segment pseudo-fits 52

Bibliography

[1] Deutsches Elektronen Synchrotron DESY. Website. `http://www.desy.de`.

[2] H1 Collaboration. *ep* Physics beyond 1999. H1 internal report H1-10/97-531, October 1997.

[3] U. Schneekloth. Recent HERA results and future prospects. DESY internal report 98-060, May 1998.

[4] I. Abt et al. The H1 detector at HERA. *Nucl. Instrum. Meth.*, A386:310–347, 1997.

[5] I. Abt et al. The tracking, calorimeter and muon detectors of the H1 experiment at HERA. *Nucl. Instrum. Meth.*, A386:348–396, 1997.

[6] T. Wolff. *Entwicklung, Bau und erste Ergebnisse eines totzeitfreien Spurfinders als Trigger für das H1-Experiment am HERA Speicherring.* PhD thesis, ETH Zürich, November 1993.

[7] A. Baird et al. A fast high resolution track trigger for the H1 experiment. *IEEE Trans. Nucl. Sci.*, 48:1276–1285, 2001.

[8] H1 collaboration. A Fast Track Trigger with high resolution for H1. Proposal submitted to the Physics Research Committee, DESY internal report PRC 99/06 and addendum PRC 99/07, 1999.

[9] S.A. Baird et al. Level 1 Fast Track Trigger - Feasibility Study. H1 internal note H1-09/99-576, April 2000.

[10] H1 Collaboration. H1 Fast Track Trigger - Specification of the L1 System. DESY report PRC 00/05, October 2000.

[11] Altera. Website. `http://www.altera.com`.

[12] D. Meer, D. Müller, J. Müller, A. Schöning, and C. Wissing. A multifunctional processing board for the fast track trigger of the H1 experiment. *IEEE Trans. Nucl. Sci.*, 49:357–361, 2002.

[13] D. Müller and J. Müller. Project H1 L2FTT Detailed Specification. Supercomputing Systems, April 2001.

[14] D. Müller, D. Meer, J. Müller, and M. Heimlicher. H1 Second Level Fast Track Trigger Design Description. Supercomputing Systems, December 2000.

[15] V. Karimäki. Effective circle fitting for particle trajectories. *Nucl. Instr. and Meth.*, A305:187, 1991.

[16] H.P. Beck. Principles and Operation of the z-Vertex Trigger. H1 internal note H1-05/96-479, 1996.

[17] D. Müller. *A Measurment of the Gluon Density in the Proton Based on Charm Production at HERA*. PhD thesis, Universität Zürich, Zürich, 1998.

[18] M. Cuje et al. H1 High Luminosity Upgrade 2000 CIP and Level 1 vertex Trigger. H1 internal note H1-01/98-535, 1998.

[19] M. Urban. Ein schneller Trigger für H1 bei HERA. Diplomarbeit, Ruprecht-Karls-Universität Heidelberg, Heidelberg, May 2000.

[20] A. Schweitzer. Optimierung eines z-Vertex-Triggers für den H1-Detektor bei HERA. Diplomarbeit, Ruprecht-Karls-Universität Heidelberg, Heidelberg, February 1999.

[21] J. Becker. H1 CIP-Vertex-Trigger upgrade - Triggerhardware-Simulation. Internal note Physikalisches Institut, Ruprecht-Karls-Universität Heidelberg, March 1998.

[22] R. Brun et al. *ROOT Users Guide 3.1c*. Geneva, September 2001.

[23] H.-C. Schultz-Coulon. private communication, June 2002.

[24] D Pitzl. private communication, June 2002.

[25] J. Samson. θ-fit in the FTT. Presentation at the FTT meeting, October 2001.